Journal of Asian Earth Sciences 164 (2018) 260–273

Contents lists available at ScienceDirect

Journal of Asian Earth Sciences

journal homepage: www.elsevier.com/locate/jseaes

Full length article

Late Cenozoic basaltic lavas from the Changbaishan-Baoqing Volcanic Belt, NE China: Products of lithosphere-asthenosphere interaction induced by subduction of the Pacific plate

Song-Yue Yu[a,*], Yi-Gang Xu[c], Sheng-Hua Zhou[a,b], Jiang-Bo Lan[a,*], Lie-Meng Chen[a], Neng-Ping Shen[a], Jian-Xin Zhao[d], Yue-Xing Feng[d]

[a] State Key Laboratory of Ore Deposit Geochemistry, Institute of Geochemistry, Chinese Academy of Sciences, Guiyang 550081, China
[b] University of Chinese Academy of Sciences, Beijing 100049, China
[c] State Key Laboratory of Isotope Geochemistry, Guangzhou Institute of Geochemistry, Chinese Academy of Sciences, Guangzhou 510640, China
[d] Radiogenic Isotope Facility, School of Earth Sciences, The University of Queensland, Brisbane, QLD 4072, Australia

ARTICLE INFO

Keywords:
Cenozoic basalt
Intraplate volcanism
Lithospheric thinning
Lithosphere-asthenosphere interaction
Northeastern China

ABSTRACT

Cenozoic intraplate basalts are low in volume but widespread in eastern China. They are predominantly alkaline and have oceanic island basalt (OIB)-like trace element compositions. Despite numerous studies, the origin of Cenozoic basalts in eastern China remains elusive. Possible roles of lithosphere thickness, subduction of Pacific plate and lithosphere-asthenosphere interaction in triggering spatial geochemical variations have not yet been clarified. Here, we have carried out mineral chemistry, major and trace element and Sr−Nd−Hf isotope analyses of the late Cenozoic (< 20 Ma) basaltic rocks from the Changbaishan-Baoqing Volcanic Belt (CVB), NE China, which revealed clear spatial compositional variations. The North CVB is dominated by basanites and alkali basalts with OIB-like trace element patterns and depleted Sr−Nd−Hf isotopic compositions ($^{87}Sr/^{86}Sr$ = 0.7039–0.7047, ε_{Nd} = 3–5.6; ε_{Hf} = 6.7–12), which may have been derived from low degree partial melting of a depleted source from asthenospheric mantle beneath a thick lithosphere. On the other hand, the South CVB consists of both alkali and sub-alkali lavas (alkali basalts, tholeiites and basaltic andesites) that display generally higher SiO_2, Sm/Nd, Ba/Nb, Th/U, and lower Nb/Th, La/Sm and more enriched Sr−Nd−Hf isotopic compositions ($^{87}Sr/^{86}Sr$ = 0.7038–0.7056, ε_{Nd} = −2.4 – +3.2; ε_{Hf} = 3–8.2). These rocks may have been produced by larger degrees of partial melting of asthenospheric mantle beneath a relatively thin lithosphere. Ancient metasomatized lithospheric mantle might also have contributed to their genesis. In addition, the similar ranges of Mn, Ni and Fe/Mn for olivine phenocrysts from both the North and the South CVB suggest that they may have been derived from hybrid mantle sources containing similar proportions of peridotite and pyroxenite/eclogite components. We propose that decompression melting of upwelling asthenosphere and mechanical-chemical erosion of basal lithosphere related to lithosphere-asthenosphere interaction responsible for the genesis of the CVB magmas were likely associated with upper mantle convection and back-arc extension induced by deep subduction of the Pacific plate and its stagnancy in the transition zone.

1. Introduction

The large compositional variations observed in intraplate basalts remain a poorly understood feature of igneous petrogenesis. Variations in magma compositions may result from the combined effects of the extent and depth of melting (e.g., McKenzie and Bickle, 1988), mantle source variation (e.g., Hofmann, 1997; Sobolev et al., 2007), and lithosphere (crust + mantle) contamination and complex magma differentiation processes (e.g., Hawkesworth et al., 1984; Arndt and Christensen, 1992). The extent and depth of melting are further controlled by variations in lithospheric thickness (e.g., Langmuir et al., 1992; Fram and Lesher, 1993; Humphreys and Niu, 2009) and mantle source lithology (peridotite vs. pyroxenite, e.g., Kogiso et al., 2003; Sobolev et al., 2005). Therefore, in order to understand the petrogenesis of intraplate basalts from a specific area or on a global scale, the effect of each of these processes should be identified.

Cenozoic basalts in eastern China are low in volume (< 10,000 km^3) and are primarily alkali basalts with minor quartz and

* Corresponding authors.
E-mail addresses: yusongyuegyig@hotmail.com (S.-Y. Yu), lanjiangbo@mail.gyig.ac.cn (J.-B. Lan).

https://doi.org/10.1016/j.jseaes.2018.06.031
Received 11 April 2018; Received in revised form 8 June 2018; Accepted 14 June 2018
Available online 19 June 2018
1367-9120/

olivine tholeiites with an oceanic island basalt (OIB)-like trace element composition and a heterogeneous isotopic signature (e.g., Basu et al., 1991; Liu et al., 1994). A high-velocity layer representative of the stagnant subducted Pacific plate in the mantle transition zone (410–660 km in depth) beneath eastern China has been imaged by P-wave tomography (e.g., Fukao et al., 1992; Huang and Zhao, 2006). Continental extension and upper mantle convection in eastern China, induced by subduction of the Pacific plate underneath the Asian continent, has been widely accepted as a possible mechanism for the genesis of the Cenozoic intraplate basaltic volcanism (e.g., Huang and Zhao, 2006; Yan and Zhao, 2008; Zhao and Ohtani, 2009; Kuritani et al., 2009, 2011, 2013; Xu et al., 2012; Sakuyama et al., 2013; Tang et al., 2014; Liu et al., 2015; Huang et al., 2015; Li et al., 2016; Tian et al., 2016; Liu et al., 2016, 2017; Li et al., 2017; Chen et al., 2017; Choi et al., 2017; Wang et al., 2017), although alternative mechanisms including upwelling of a mantle plume (Wang et al., 2012, 2013, 2015; Yu et al., 2015a,b) or eastward asthenospheric flow from beneath western China to eastern China (Niu, 2005; Guo et al., 2014) also have been proposed. Previous studies also demonstrated that the Cenozoic basalts from North and northeastern China are dominated by mixing of the depleted MORB source mantle (DMM) and the EM1 ("Enriched Mantle"-1, as defined by Zindler and Hart, 1986) components (e.g., Zhang et al., 1995; Yan and Zhao, 2008; Kuritani et al., 2011, 2013; Zeng et al., 2011; Li et al., 2016), whereas those from South China are dominated by EM2 ("Enriched Mantle"-2) and DMM components (e.g., Zou et al., 2000; Huang et al., 2013). The origin of these mantle source components is still controversial. Some authors suggested that the DMM and EM1 components were derived from typical asthenospheric mantle peridotite and ancient metasomatized peridotite in the sub-continental lithospheric mantle (SCLM), respectively (Zhang et al., 1995; Okamura et al., 2005; Yan and Zhao, 2008). Others proposed that the DMM mantle component consists of carbonated peridotites or pyroxenites (Zeng et al., 2010, 2011, 2017; Yang et al., 2012; Tian et al., 2016; Li et al., 2016; Li et al., 2017). The EM1 mantle component may represent recycled lower continental crust (Chen et al., 2009; Zeng et al., 2010, 2011) or ancient garnet pyroxenite within the asthenosphere (Li et al., 2016). In addition, some other authors argued that the EM1 mantle component consists of ancient marine sediments related to ancient subduction (Kuritani et al., 2011, 2013; Liu et al., 2015; Wang et al., 2017).

The Changbaishan-Baoqing Volcanic Belt (CVB), the northern part of the Cenozoic intraplate volcanic belt in eastern China, consists of numerous volcanoes with ages ranging from 49 Ma to recent. The CVB was largely associated with the activation and development of the Fushun-Mishan fault (Liu et al., 1992a, Fig. 1). The lithospheric thickness beneath the South CVB is between 60 and 80 km (Fig. 1c, Zheng et al., 2011), and it is between 100—120 km beneath the north CVB (Fig. 1c, Zhang et al., 2014). The depth of the LAB (lithosphere-asthenosphere boundary) is estimated from SRFs (S-wave receiver functions) as the median depth among the ten most negative values in the vertical CCP (common conversion point) profiles (Zhang et al., 2014). Given the difference in lithospheric thickness in this region, basaltic lavas in the CVB may display spatial compositional variation because the lithospheric thickness controls the final pressure of decompression melting and the corresponding depth defines the bulk distribution coefficients of elements in the source, which ultimately governs the geochemistry of intraplate basalts (Niu et al., 2011; Humphreys and Niu, 2009). However, previous studies about this volcanic belt mainly focused on the genesis of basalts from an individual volcanic field, such as Jingbohu and Changbaishan (Yan and Zhao, 2008; Kuritani et al., 2009, 2011). For example, Yan and Zhao (2008) considered that the source of the Jingbohu alkali basalts contains an EM1 component which is likely derived from the lithospheric mantle due to lithosphere-asthenosphere interaction. In contrast, Kuritani et al. (2009, 2011) argued that the EM1 mantle component in the source of the Changbaishan basalts is possibly derived from the ancient subducted oceanic slab in the mantle transition zone. Spatial compositional variation for the CVB basalts has not been reported before.

In order to better understand the spatial compositional variation for the CVB lavas and their possible origins, we carried out an integrated olivine chemical and whole-rock chemical and Sr—Nd—Hf isotopic study of the CVB basaltic samples from Northeastern China. Based on integration of our geochemical data with available geophysical information, a new tectonomagmatic model was proposed to account for the generation of these CVB basaltic lavas.

2. Geological background and sampling

2.1. Geological background

Northeast China is composed of two major tectonic units, the Xing'an Mongolian Orogenic Belt (XMOB) in the north, and the North China Craton (NCC) in the south (Fig. 1a). The NCC is one of the oldest tectonic units in China, preserving crustal rocks as old as 3.8 Ga (Liu et al., 1992b). The XMOB is the eastern part of the Paleozoic Central Asian Orogenic Belt, which is considered as a composite fold belt that underwent collision and subduction between the NCC and the Siberian Craton (Jahn et al., 2000). Since the late Mesozoic Era, NE China became an important part of the circum-Pacific tectonic-magmatic belt. During this stage, intensive deformation, mineralization, and igneous activity occurred, including extensive eruption of intermediate-acid volcanic rocks and wide-scale emplacement of granites. During the Cenozoic Era, intraplate volcanism was widespread in northeastern China and adjacent areas although volumetrically small. In an area of about two million square kilometers, over 590 volcanoes developed, emplacing basaltic rocks over an area of about 50000 km^2 (Fig. 1a, Liu, 1999; Ma et al., 2002). The erupted products have been grouped into three successive episodes: (1) late Cretaceous-Paleogene sub-alkaline and alkaline basalts; (2) Neogene alkali basalts with minor tholeiitic basalts, and (3) Quaternary alkaline basalts (Fan and Hooper, 1989). Individual lava flows are typically massive and aphyric or porphyritic at base and gradually become vesicular to top. Mantle xenoliths, mainly spinel lherzolite and harzburgite, are mostly found in the Neogene and Quaternary alkaline basalts and are generally lacking in the tholeiitic flows. These peridotite mantle xenoliths are mainly anhydrous and lack metasomatic phases such as amphibole and phlogopite. Numerous studies have been conducted on these rocks (e.g., Basu et al.,1991; Tatsumoto et al.,1992; Zhang et al., 2000; Xu et al., 1998, 2003; Wu et al., 2003; Yu et al., 2009, 2010, 2012). Peridotite xenoliths are essentially Proterozoic in age according to their Re-Os isotopic compositions (Wu et al., 2003). They are considered to be ancient melting residues that have experienced later pervasive metasomatism (Tatsumoto et al., 1992; Zhang et al., 2000; Xu et al., 1998, 2003; Yu et al., 2009, 2012). The CVB mainly consists of five volcanic fields (Baoqing, Mudanjiang, Laoheishan, Dunhua and Changbaishan, Fig. 1b). Detailed description of lavas in these volcanic fields is shown in Electronic Appendix 1.

2.2. Samples and their petrography

The basaltic samples used in this study were collected from eleven different locations in five volcanic fields (Baoqing, Mudanjiang, Laoheishan, Dunhua and Changbaishan, Fig. 1b). These samples are massive and generally fresh with K-Ar or Ar-Ar ages ranging from 16.4 to less than 1 Ma (Electronic Appendix 2, Liu, 1987, Liu et al., 1992a, Wang et al., 2003, Wei et al., 2007, Qin, 2008). Our basaltic samples are classified primarily based on the total alkali versus silica (TAS) diagram (Fig. 2, Le Bas et al., 1986). Samples from the Baoqing and Mudanjiang volcanic fields in the north part of the CVB mostly plot within the alkaline series field. They are compositionally basanite to alkaline basalt. In contrast, samples from the Laoheishan, Dunhua and Changbaishan volcanic fields in the south part of the CVB plot within both the alkaline

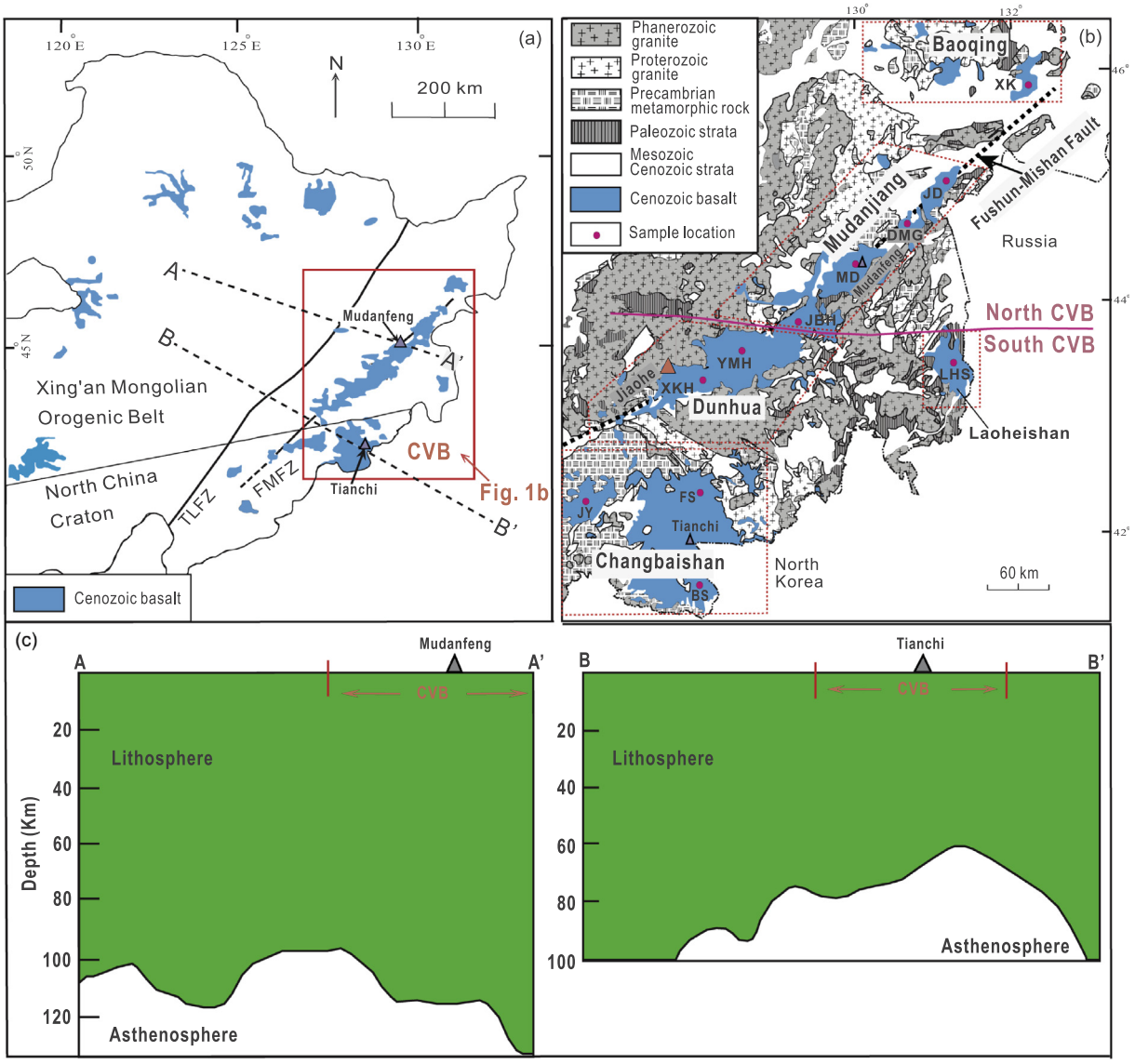

Fig. 1. (a) Simplified tectonic scheme and distribution of Cenozoic basalts in northeastern China. The Cenozoic basalts in the red box belong to the Changbaishan-Baoqing Volcanic Belt (CVB). (b) The distribution of the Cenozoic basalts in the CVB. The CVB mainly consists of five volcanic fields (Baoqing, Mudanjiang, Laoheishan, Dunhua and Changbaishan). Basaltic samples were collected from different locations: BS (Baishan), JY (Jingyu), FS (Fusong), LHS (Laoheishan), YMH (Yanminghu), XKH (Xinkaihe), JBH (Jingbohu), MD (Mudanfeng), DMG (Daimagou), JD (Jidong), XK (Xingkai). TLFZ (Tanlu fault zone), FMFZ (Fushun-Mishan fault zone). The red triangle represents the sample location for the Jiaohe garnet pyroxenite. (c) Estimated lithospheric thickness along the lines shown in Fig. 1a (modified after Zheng et al., 2011; Zhang et al., 2014).

series and sub-alkaline series fields. They display variable kinds of lithological types (including alkaline basalt, tholeiite and basaltic andesite). Given the spatial difference in lithological type, basaltic samples from the CVB are divided into the two groups of “North CVB” and “South CVB” (Fig. 2). Alkaline lavas from the Baoqing and Mudanjiang volcanic fields belong to the “North CVB” group. Alkaline and sub-alkaline lavas from the Laoheishan, Dunhua and Changbaishan volcanic fields belong to the “South CVB” group. Basanites from the North CVB have high normative nepheline (10–17%), in contrast to generally low normative nepheline (< 10%) in alkali basalts (Electronic Appendix 2). In addition, normative nepheline is absent in tholeiites and basaltic andesites from the South CVB. Basaltic andesites from the South CVB contain normative quartz (Electronic Appendix 2).

The basanites and alkali basalts from the North CVB and the South CVB show similar dark green color and porphyritic texture (Fig. 3a and b), and consist of 2–5% small subhedral olivine phenocrysts (0.1–0.5 mm in diameter) and minor clinopyroxene. The groundmass is composed of fine-grained olivine, plagioclase, clinopyroxene and minor Fe—Ti oxides. The tholeiites from the South CVB have 5–10% olivine and clinopyroxene phenocrysts and minor plagioclase in a groundmass of olivine, plagioclase, clinopyroxene and minor Fe-Ti oxides (Fig. 3c). Olivine phenocrysts are subhedral to anhedral (0.5–2 mm in diameter). Some olivine phenocrysts are partially altered to iddingsites leaving fresh core as relicts. The basaltic andesites from the South CVB consist of 10–15% clinopyroxene and plagioclase and minor olivine phenocrysts (Fig. 3d). Plagioclase phenocrysts are tabular (0.5–1 mm). Polysynthetic twinning is common in the plagioclase. The groundmass is composed of fine-grained plagioclase, clinopyroxene and minor Fe—Ti oxides.

3. Sample preparation and analytical methods

Concentrations of major elements in whole rocks were determined using a PANalytical Axios X-ray fluorescence spectrometer (XRF) on

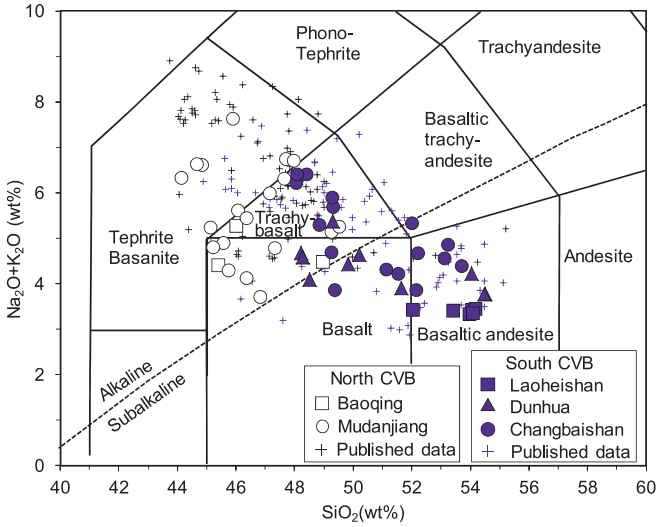

Fig. 2. Total alkali versus silica (TAS) diagram for the Cenozoic CVB lavas (Le Bas et al., 1986). Line separating alkali and subalkaline series is from Irvine and Baragra (1971). Published data of the North and the South CVB basaltic lavas are from Liu et al. (1994), Hsu and Chen (1998), Hsu et al. (2000), Zhang et al. (2002) and Chen et al. (2007), Yan and Zhao (2008), Kuritani et al. (2009).

fused glass beads in the laboratory of ALS (Analytical chemistry & testing services) Chemex Ltd in Guangzhou, China. A 0.7 g powder sample was mixed completely with $Li_2B_4O_7$–$LiBO_2$ flux and then fused to a glass bead at 1050–1100 °C. Loss on ignition (LOI) was determined by heating a 1 g powder sample to 1100 °C for 3 h. The analytical errors were mostly < 5% (Electronic Appendix 2).

Trace element and Sr–Nd–Hf isotope analyses were performed at the Radiogenic Isotope Facility, School of Earth Science, the University of Queensland, Australia. Approximately 60 mg of each rock powder was dissolved in Savillex™ Teflon bombs with a distilled HF-HNO_3 mixture. The dissolution was maintained in an oven at 185 °C for 3 days. The solutions were then dried down to evaporate HF. Sample residues were re-dissolved with concentrated HNO_3 followed by 1:1 HNO_3 and dried again. Finally, the samples were dissolved in a final 3 ml 2 N HNO_3 stock solution. Sample solutions were mixed with 6 ppb ^{6}Li, ^{61}Ni, Rh, In, Re, and ^{235}U internal spikes and diluted with 2% HNO_3 to achieve a final dilution factor of about 1:4000 for trace element analysis. The abundances of trace elements were determined using a Thermo X Series II ICP-MS following the protocol of Eggins et al. (1997). USGS standard W2 was used as a calibration standard and cross-checked with BIR-1. Standards BHVO-2, BCR-2 and W-2a were determined as unknowns. The overall analytical precision is better than 3% relative to the certified values (Electronic Appendix 3, GeoReM: http://georem.mpch-mainz.gwdg.de/).

Isotope ratios for Sr, Nd and Hf were obtained on the remaining stock solution aliquots left from the trace element analyses. Sr, Nd and Hf chemical separations were performed following a modified procedure described by Pin and Zalduegui (1997), Deniel and Pin (2001) and Míková and Denková (2007). Strontium was separated from other elements using Sr-Spec resin and deposited on Ta filaments with TaF_5, and isotope ratios were measured on a VG Sector 54 thermal ionization mass spectrometer (TIMS). The NBS-987 standard was used as a monitor of the detector efficiency drift of the instrument. It was repeatedly measured during the analysis of the samples (n = 45) and yielded an average of 0.710222 ± 20 (2σ). The deviation of this mean value from the laboratory's previously obtained long-term average of 0.710249 ± 28 (2σ) was used for data correction.

Neodimium was separated using Ln-Spec resin, and isotope ratios were analyzed on a Nu Plasma multi-collector inductively coupled plasma mass spectrometer (MC-ICPMS). Instrumental bias and mass fractionation were corrected by normalizing raw ratios to $^{146}Nd/^{144}Nd = 0.7219$. Accuracy was tested by analyzing the JNdi-1, BCR-2 and BHVO-2 USGS rock standards. The JNdi-1 standard yielded $^{143}Nd/^{144}Nd = 0.512113 \pm 9$ (2σ, n = 11), consistent with the expected value: 0.512115 ± 7 (Tanaka et al., 2000). The BCR-2 standard yielded $^{143}Nd/^{144}Nd = 0.512629 \pm 6$ (2σ, n = 3), consistent with the expected value of 0.512635 ± 29 (GeoReM: http://georem.mpch-mainz.gwdg.de/), and BHVO-2 yielded $^{143}Nd/^{144}Nd = 0.512977 \pm 6$ (2σ, n = 2), matching the certified value of 0.512979 ± 14 (GeoReM: http://georem.mpch-mainz.gwdg.de/).

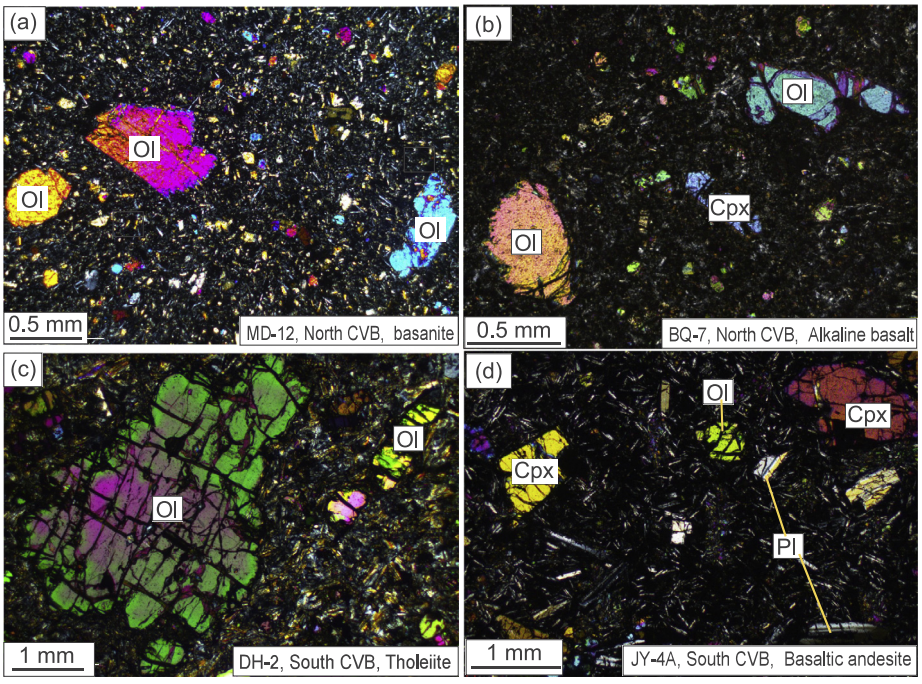

Fig. 3. Crossed-polarizers representative photomicrographs for the investigated rock samples from the North and the South CVB. Ol = olivine, Cpx = clinopyroxene, Pl = plagioclase.

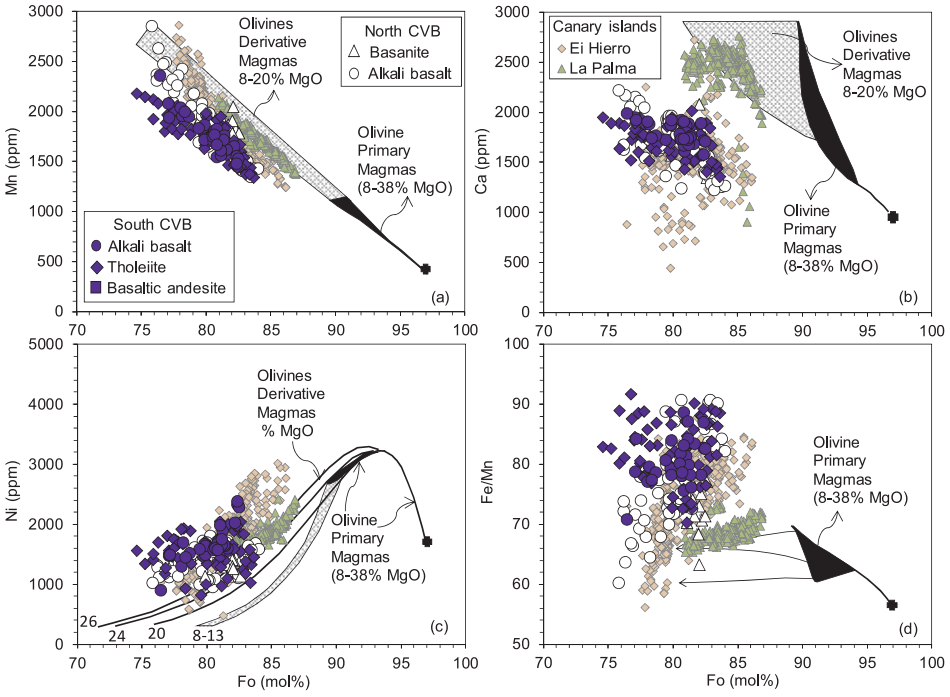

Fig. 4. Plots of Mn, Ca, Ni and Fe/Mn vs. Fo for olivine phenocrysts from the Cenozoic basalts of the CVB. The data for olivine phenocrysts from EI Hierro and La Palma basalts from the Canary Islands, Spain (Gurenko et al., 2009) and those for olivine grains crystallized from peridotite-derived melts calculated following the procedure reported in the Herzberg (2011) are also shown for comparison. The calculation was based on a fertile peridotite source with 8.02% FeO, 1964 ppm Ni, 24657 ppm Ca, and 1007 ppm Mn. Calculated olivines are for both primary magmas and derivative liquids produced by olivine fractionation. The filled black fields are for olivines from primary magmas, the numbered lines and fields are for olivines from derivative liquids produced by olivine fractionation. The numbers represent MgO contents of derivative magmas. Left pointing arrows in Fig. 4d are examples of olivines in derivative melts produced by olivine fractionation of primary magmas.

The measurement of Hf isotope ratios was conducted on a Nu Plasma HR MC-ICP-MS. 10 ppm Hf ICP solution from Choice Analytical was used as the instrument drift monitor. This in-house standard was cross-calibrated against the JMC-475 Hf international standard through parallel bracketing measurements. Its repeated measurements yielded an average $^{176}Hf/^{177}Hf$ of 0.282145 ± 6 (n = 16, 2SD), corresponding to an average value of 0.282160 ± 6 (n = 16, 2SD) for the JMS-475 standard. The in-house Hf standard monitor was measured between every 5 samples and 37 repeated measurements gave an average $^{176}Hf/^{177}Hf$ value of 0.282133 ± 3 (2SD), which was used to correct instrumental drift on measured sample ratios relative to the JMS-475 Hf standard. Accuracy was assessed by analyzing the BHVO-2 USGS rock standard. The BHVO-2 yielded $^{176}Hf/^{177}Hf$ = 0.283096 ± 4 (2σ, n = 2), matching the certified value of 0.283082 ± 133 (GeoReM: http://georem.mpch-mainz.gwdg.de/).

The chemical compositions of olivine and clinopyroxene grains were determined by wavelength-dispersive X-ray emission microanalysis using a CAMECA SX50 electron microprobe in the Department of Geological Sciences at Indiana University. Analytical conditions for major elements were a 15 keV accelerating voltage, a 20 nA beam current, a 1 μm beam size and a peak counting time of 20 s. Minor elements (Ca, Mn and Ni) in olivine were analyzed using a beam current of 100 nA and a peak counting time of 100 s. Under these conditions the detection limits were estimated to be 20 ppm Ca, 60 ppm Mn and 80 ppm Ni. Matrix effects were corrected using the PAP program supplied by CAMECA. The accuracy of the analyses was monitored using mineral standards, and analytical uncertainty was within ± 2% of accepted values.

4. Results

4.1. Mineral composition

The chemical compositions of olivine in Cenozoic basalts from the CVB are listed in Electronic Appendix 4. CaO contents of olivine cores are typical of magmatic values (0.17–0.3 wt%, Electronic Appendix 4), significantly higher than those of mantle peridotite xenoliths in this region (< 0.1 wt%, Xu et al., 2003; Yu et al., 2009), and Fo contents of olivine cores are lower (75–84) than those of mantle peridotite xenoliths (> 89, Xu et al., 2003; Yu et al., 2009). Along with the presence of euhedral and subhedral shapes and lack of strain textures, all these features indicate that olivine grains in the Cenozoic basalts from the CVB represent phenocrysts that crystallized from melt rather than mantle xenocrysts. Chemical zoning is common in olivine phenocrysts from both the North and the South CVB with Fo decreasing from core to mantle and rim (Electronic Appendix 4). No clear chemical distinction between the South and the North CVB olivine phenocrysts from the same lithological type was observed in this study. For example, cores of olivine phenocrysts in alkali basalts from the North and the South CVB have similar ranges of Fo (76–84 and 76–83, respectively). Cores of olivine phenocrysts in tholeiites and basaltic andesites from the South CVB also have a comparable range of Fo (74–83). Moreover, at a given Fo, olivine cores from the North and the South CVB display similar ranges of Mn, Ca, Ni contents and Fe/Mn ratios (Fig. 4), regardless of lithological type. Mn and Ca contents of the CVB samples are negatively correlated with Fo (Fig. 4a and b). Ni decreases with decreasing Fo (Fig. 4c). It is noted that Fo of olivine cores (74–79) is slightly lower in some samples (e.g., CBS-28 and JY-4A, Electronic Appendix 4) and that clinopyroxene and plagioclase phenocrysts are much more abundant than olivine.

4.2. Whole-rock chemical composition

Whole-rock major and trace element and Sr-Nd-Hf isotope compositions of the CVB basalts are listed in Electronic Appendix 2. The CVB basaltic rocks have variable MgO contents (4.5–11.5 wt%) and Mg# ($Mg/(Mg + 0.85 \times Fe^{total}) \times 100$, 47–70). Al_2O_3, CaO, Ni and Sc contents and CaO/Al_2O_3 ratios in the CVB basaltic samples correlate positively or negatively with Mg# (Fig. 5). Basanites and alkali basalts generally have lower SiO_2 and higher CaO, $Fe_2O_3^T$, and TiO_2 than tholeiites and basaltic andesites (Fig. 5). Specifically, alkali basalts and basanites from the North CVB have relatively high Mg# (54–66). In contrast, alkali basalts from the South CVB have variable Mg# (47–67). Tholeiites and basaltic andesites from the South CVB also have variable Mg# (49–70). At a given Mg#, alkali basalts from the North CVB display slightly lower SiO_2 and higher Fe_2O_3T than alkali basalts from the South CVB (Fig. 5a and d).

In the primitive-mantle normalized incompatible trace element

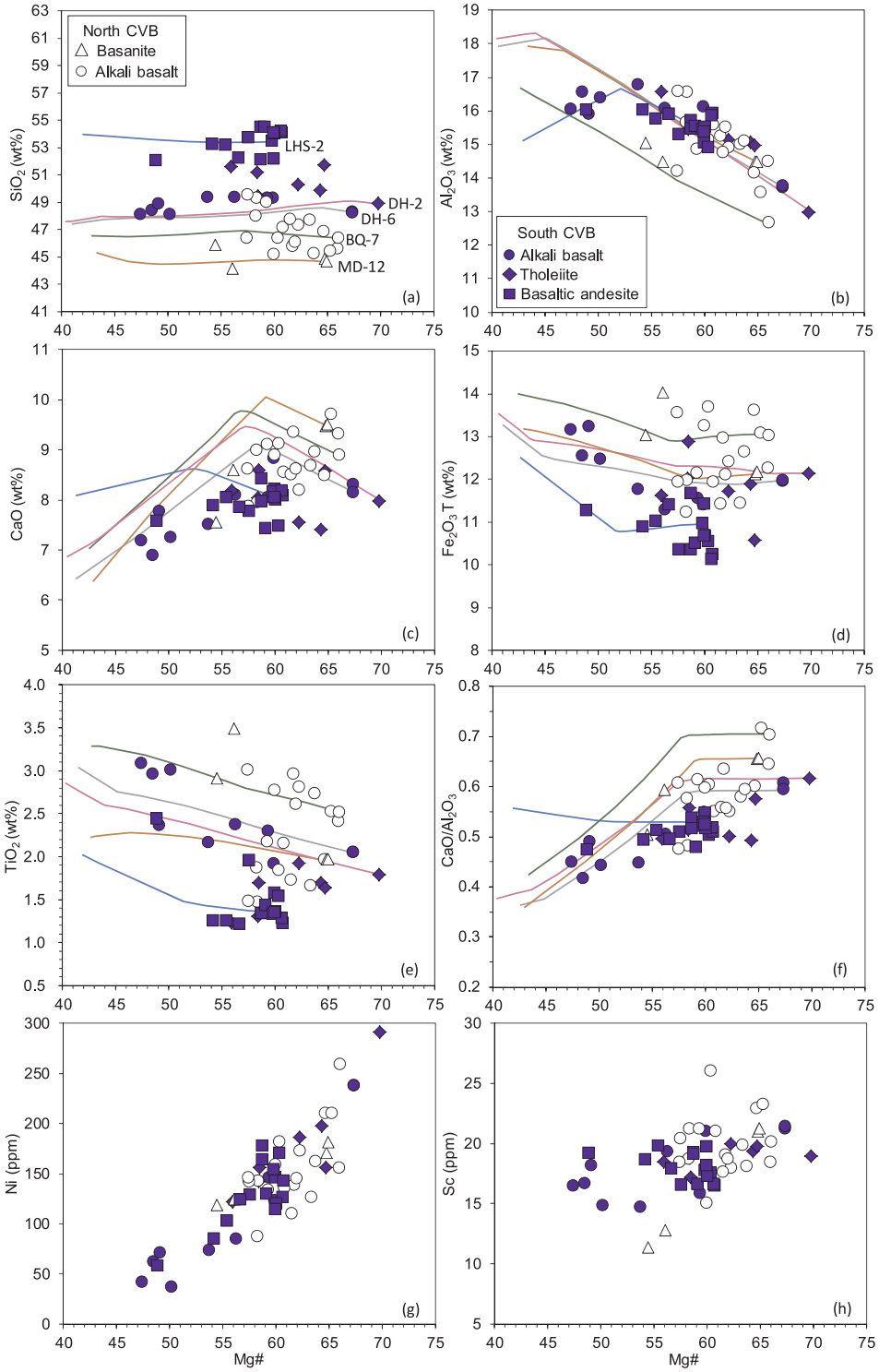

Fig. 5. Diagrams of major and trace element contents and ratios vs. Mg# (molar Mg/(Mg + Fe^{2+}) × 100) for the CVB basaltic lavas. Five solid lines in different colors represent modeled fractional crystallization paths of two Mg-richer samples from the North CVB (MD-12 and BQ-7) and three Mg-richer samples from the South CVB (DH-6, DH-2 and LHS-2) in a water-free system at 5 kbar and fO_2 = QFM using the MELTS program of Ghiorso and Sack (1995). See text for more detailed information.

diagrams (Fig. 6), samples from the North CVB are strongly enriched in LILE (Large Ion Lithophile Elements) with peaks at Nb and Ta, similar to typical OIB (Fig. 6a). In contrast, basalts from the South CVB display variable degrees of LILE enrichment (e.g., Rb, Ba and K) and HFSE (High Field Strength Element, e.g., Nb, Zr, Hf and Ti) depletion (Fig. 6b). Specifically, basanites and alkali basalts from the North CVB display similarly low Rb/Nb (0.25–0.93), Ba/Nb (6.8–14.5) and Th/Nb (0.07–0.11) (Electronic Appendix 2)). Alkali basalts and tholeiites from the South CVB show similarly intermediate Rb/Nb (0.51–1.34), Ba/Nb (8.6–29.3) and Th/Nb (0.08–0.16) (Electronic Appendix 2)). Basaltic andesites from the South CVB show the highest Rb/Nb (0.61–2.72), Ba/Nb (16–46.8) and Th/Nb (0.11–0.22). In addition, basanites and alkali basalts from the North CVB display similarly high La/Sm (4.5–7.5), Zr/Zr* ($(Zr_n/(Sm_n \times Nd_n)^{0.5}$), 0.9–1.7), and low Th/U (2.5–5.3), Sm/Nd

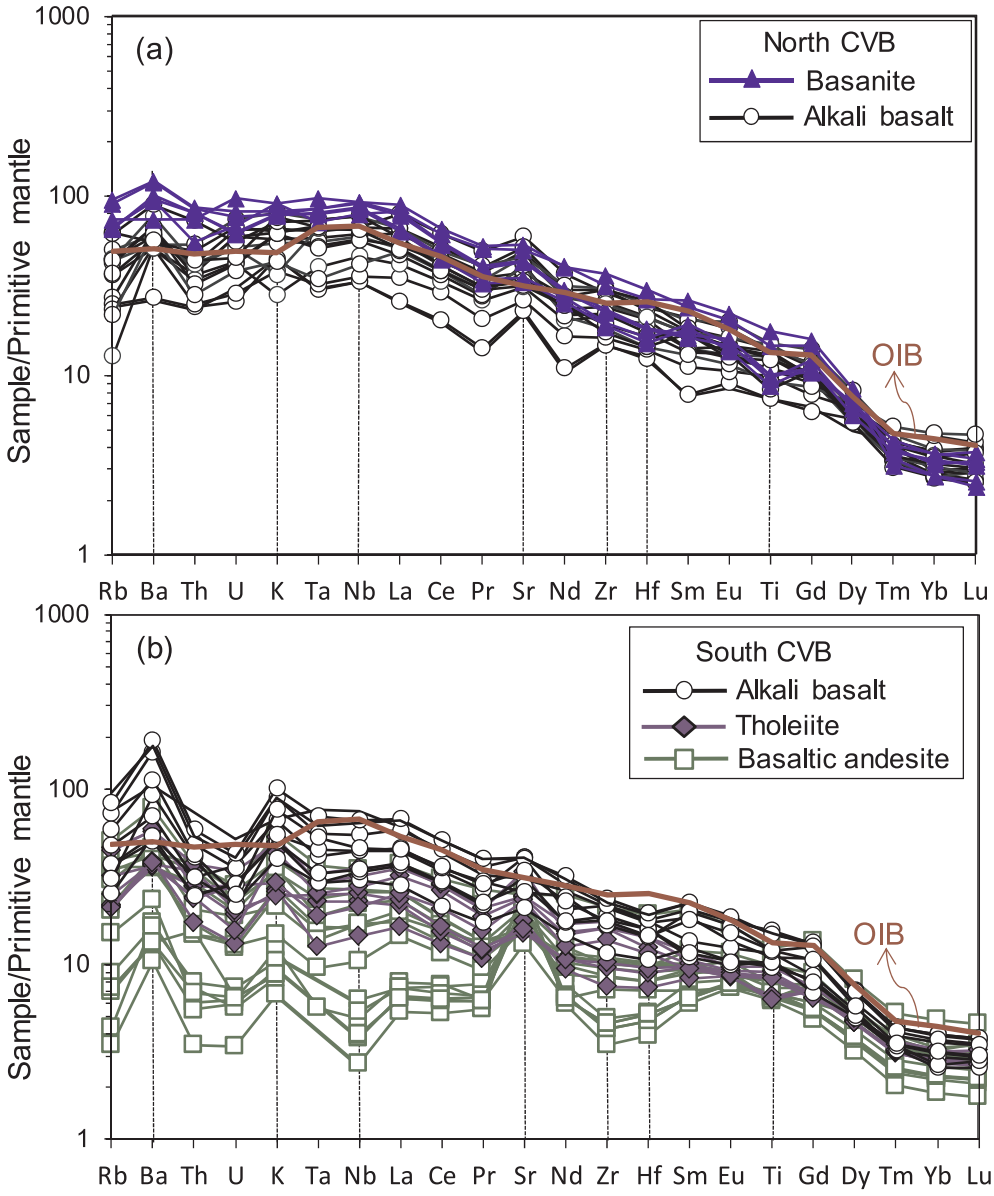

Fig. 6. Primitive mantle-normalized incompatible element patterns of the CVB basaltic lavas. Normalization values and the pattern for a typical OIB (red color) are from Sun and McDonough (1989).

(0.18–0.24). In contrast, alkali basalts and tholeiites from the South CVB show similarly intermediate La/Sm (2.5–5.9), Zr/Zr^* (0.8–1.3), Th/U (3.4–8.8), Sm/Nd (0.21–0.31). Basaltic andesites from the South CVB show the lowest La/Sm (1.4–4.0), Zr/Zr^* (0.6–1.1), and the highest Sm/Nd (0.27–0.36) (Electronic Appendix 2)).

The Sr, Nd and Hf isotope compositions of Cenozoic basalts from the CVB plot within the MORB and OIB field and define a negative correlation in the Sr—Nd isotopic plot (Fig. 7a) and a positive correlation in the Nd—Hf isotopic plot (Fig. 7b). Specifically, basanites and alkali basalts from the North CVB display a rather uniform Sr—Nd—Hf isotopic composition ($^{87}Sr/^{86}Sr$ = 0.7038–0.7047, $^{143}Nd/^{144}Nd$ = 0.5127–0.5129, $^{176}Hf/^{177}Hf$ = 0.2830–0.2831). Samples from the South CVB display similarly higher $^{87}Sr/^{86}Sr$ (0.7038–0.7054), lower $^{143}Nd/^{144}Nd$ (0.5125–0.5128) and $^{176}Hf/^{177}Hf$ (0.2828–0.2830), regardless of lithological type (Fig. 7).

5. Discussion

The late Cenozoic CVB basaltic samples in this study display clear spatial difference in lithological types: The North CVB (including the Baoqing and Mudanjiang volcanic fields), where the lithosphere is relatively thick (100–120 km, Fig. 1c, Zhang et al., 2014), is dominated by alkali lavas (basanites and alkali basalts, Fig. 2), whereas the South CVB (including the Dunhua, Laoheishan and Changbaishan volcanic fields), where the lithosphere is thinner than 80 km (Fig. 1c, Zheng et al., 2011), includes both alkali and sub-alkali lavas (basanites, alkali basalts, tholeiites and basaltic andesites, Fig. 2). Previous studies also have demonstrated that late Cenozoic basaltic samples collected from the Mudanjiang volcanic field in the North CVB are primarily basanites and alkali basalts (Hsu and Chen, 1998; Zhang et al., 2002; Chen et al., 2007; Yan and Zhao, 2008, Fig. 2). Basaltic samples from the Changbaishan and Laoheishan volcanic fields in the South CVB consist of basanites, alkali basalts, tholeiites and basaltic andesites (Hsu et al., 2000; Chen et al., 2007; Qin et al., 2008; Kuritani et al., 2009, Fig. 2). All these observations support our speculation that there is clear distinction in lithological types between the North and the South CVB basaltic lavas, although sampling bias cannot be totally excluded. In addition, the North CVB basalts display relatively constant depleted

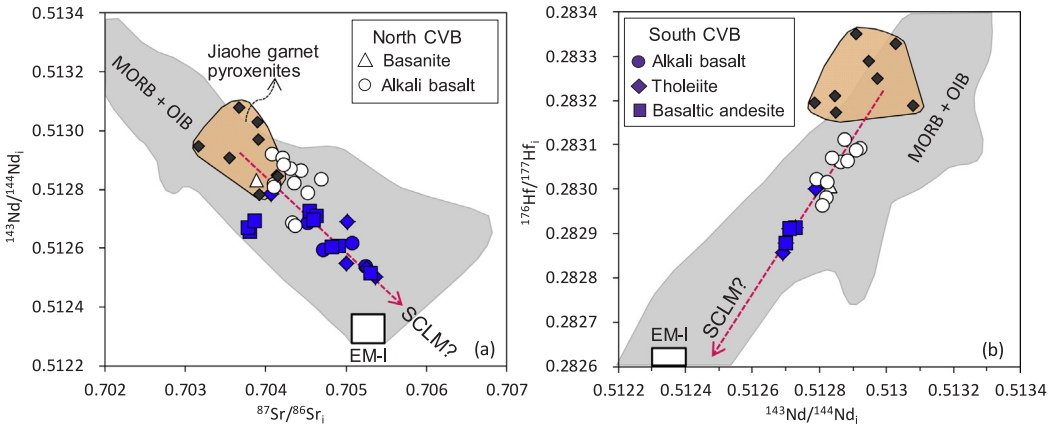

Fig. 7. Whole-rock $^{143}Nd/^{144}Nd$ vs. $^{87}Sr/^{86}Sr$ and $^{176}Hf/^{177}Hf$ for the CVB basaltic lavas. Data for the Jiaohe garnet pyroxenites are from Yu et al. (2010) and this study (Electronic Appendix 5). Mid-Ocean Ridge Basalt (MORB) and Ocean Island Basalt (OIB) and Enriched Mantle I (EM-I) end-member compositions are after Hofmann (1997), Ballentine et al. (1997) and Chauvel and Blichert-Toft (2001).

Sr–Nd–Hf isotopic compositions, whereas samples from the South CVB demonstrate largely variable Sr–Nd–Hf isotopic compositions from depleted to enriched (Fig. 7). Any viable petrogenetic models proposed should be able to account for such lithological and compositional differences between basalts from the North and the South CVB. Several possible parameters include (1) post-magmatic alteration and crystal fractionation, (2) crustal contamination and mantle source heterogeneity, and (3) the influence of lithosphere thickness. The role of these parameters and processes in the genesis of the late Cenozoic basalts in the North and the South CVB will be discussed below.

5.1. Post-magmatic alteration and crystal fractionation

The basaltic samples from the CVB are Neogene to Quaternary in age (< 20 Ma) and are generally very fresh, as indicated by the observation of fresh phenocrysts and matrix (Fig. 3), low loss on ignition (LOI) values (mostly below 1 wt%, Electronic Appendix 2) and lack of correlation between LOI and fluid-mobile elements (such as Rb, Ba, Sr, Pb, U, not shown). More importantly, post-magmatic hydrothermal alteration cannot explain the chemical differences between the North and the South CVB basaltic samples because they have similar ranges of LOI (−0.2 – +4.4 wt% and −0.6 – +4.3 wt%, respectively, Electronic Appendix 2).

Basaltic samples from the South CVB have experienced variable degrees of crystal fractionation. This is reflected by wide ranges of Mg# (47–70), Cr (35–346 ppm) and Ni contents (37–290 ppm, Fig. 5g), all of which are remarkably lower than those of primary magmas (i.e., Mg# = 68–75, Cr > 1000 ppm, Ni > 500 ppm, Frey et al., 1978), although variation of the Cr and Ni contents are also partially related to possible incorporation of olivine or pyroxene phenocrysts during powder making processes. Moreover, Fo of olivine phenocrysts (76–84) is significantly lower with respect to primitive olivine (Fo90) in equilibrium with primary basaltic magmas. In contrast, basaltic samples from the North CVB have experienced lesser crystal fractionation, as indicated by narrower ranges of Mg# (54–66), Cr (98–314 ppm) and Ni contents (88–260 ppm, Fig. 5g). To further evaluate the effects of crystal fractionation, we simulated the fractional crystallization paths of two Mg-richer samples from the North CVB (MD-12 (basanite, Mg# = 65), BQ-7 (alkali basalt, Mg# = 66)) and three Mg-richer samples from the South CVB (DH-6 (alkali basalt, Mg# = 67), DH-2 (tholeiite, Mg# = 70), LHS-2 (basaltic andesite, Mg# = 60)) in a water-free system at 5 kbar and fO_2 = QFM using the MELTS program of Ghiorso and Sack (1995). The modeled mineral crystallization sequences of basaltic samples from the North CVB are different from those from the South CVB (Fig. 5). For basanites and alkali basalts from the North CVB (e.g., MD-12, BQ-7), olivine is the first silicate phase on the liquidus, followed by clinopyroxene and then plagioclase. This is generally consistent with petrographic observations. For example, olivine is the dominant phenocryst in the Mg-richer samples (e.g., MD-12, BQ-7, Fig. 3a and b). More abundant clinopyroxene phenocrysts are observed in relatively evolved melts (e.g., MD-3, not shown). Fe_2O_3T and TiO_2 contents of residual melts increase during fractional crystallization (Fig. 5d and e), while SiO_2 contents keep nearly constant (Fig. 5a). Early crystallization of olivine results in increasing Al_2O_3 and CaO in residual melts with decreasing Mg# (Fig. 5b and c), and then crystallization of clinopyroxene accounts for sharply decreasing CaO and CaO/Al_2O_3 in residual magmas (Mg# < 58, Fig. 5c and f). In contrast, for alkali basalts from the South CVB (e.g., DH-6), the sequence of mineral crystallization is: olivine → orthopyroxene → clinopyroxene → plagioclase. Tholeiites and basaltic andesites (e.g., DH-2, LHS-2) from the South CVB display a crystallization sequence similar to that of the above alkali basalts. This is partially consistent with petrographic observations. Mg-richer samples (e.g., DH-2 and DH-6) contain abundant olivine phenocrysts with minor clinopyroxene (Fig. 3c). Samples with low Mg# have more abundant clinopyroxene and plagioclase (e.g., JY-4A, Fig. 3d). However, no orthopyroxene phenocryst is observed in the basaltic samples from the South CVB. In general, most samples from the CVB follow the modeled fractionation paths. Variations of major element and some trace element (e.g., Ni and Sc) contents with decreasing Mg# for the CVB samples (Fig. 5) can be readily explained by variable degrees of fractional crystallization of olivine and pyroxene. It should be pointed out that, at a given Mg#, generally higher SiO_2 and lower Fe_2O_3T for samples from the South CVB than those from the North CVB (Fig. 5a and d) cannot be explained by fractional crystallization, but may simply be attributed to more abundant sub-alkali lavas (tholeiites and basaltic andesites) in the South CVB.

5.2. Crustal contamination versus mantle source heterogeneity

Most CVB samples underwent insignificant crustal contamination, regardless of lithological types. This is supported by their oceanic basalt-like Nb/U ratios and lack of correlation between MgO/SiO_2 and Nb/U (Fig. 8a), and between Mg# and $(La/Nb)_n$ (Fig. 8b). This is also supported by lack of correlation between ε_{Nd} and Nb/U (Fig. 8c) and $(La/Nb)_n$ (Fig. 8d). However, eight basaltic andesitic samples and one tholeiitic sample from the South CVB show abnormally low Nb/U (19–30) and high $(La/Nb)_n$ (1.2–2.0). These samples have experienced significant crustal contamination and will be excluded in further discussions.

Sobolev et al. (2005, 2007) used the composition of olivine phenocrysts to evaluate the importance of magma derivation from a peridotitic mantle source relative to that of a pyroxenitic (recycled eclogitic

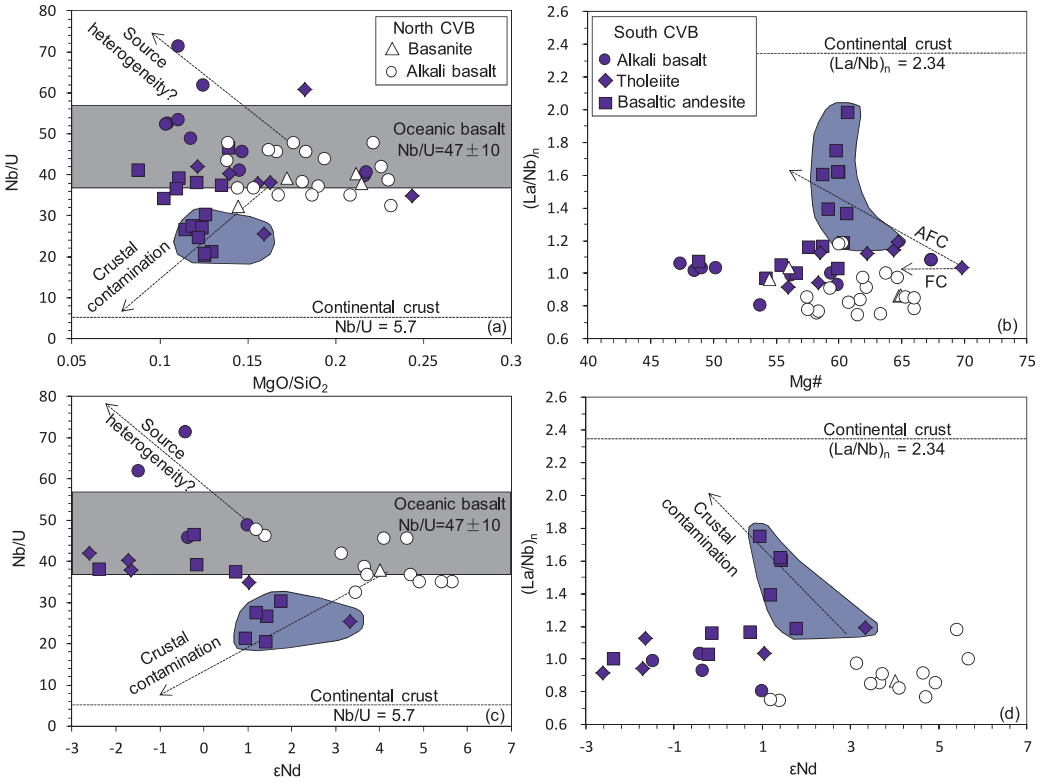

Fig. 8. Plots of MgO/SiO_2 vs. Nb/U (a), Mg# vs. $(La/Nb)_n$ (b), ε_{Nd} vs. Nb/U and $(La/Nb)_n$ (c and d) for the CVB basaltic lavas. Most basaltic samples from the CVB have Nb/U ratios similar to those of oceanic basalts (37–57, Hofmann et al., 1986) with little correlation with MgO/SiO_2 or ε_{Nd}, indicating insignificant crustal contamination. It is noted that nine samples have much lower Nb/U (19–30) and higher $(La/Nb)_n$ (1.2–2.0) than the other samples, indicating significant assimilation of continental crust with low Nb/U and $(La/Nb)_n$ (5.7 and 2.34, respectively, Rudnick and Fountain, 1995).

material) source. The method employed was based primarily on the NiO, MnO and CaO contents of the olivine phenocrysts. At a given Fo, olivine phenocrysts from the CVB basaltic samples display significantly lower Mn, Ca, but higher Ni, Fe/Mn, relative to the calculated compositions of olivine phenocrysts crystallized from the peridotite-derived melts (Fig. 4). This can be explained by a significant pyroxenite component in the source region of the CVB basalts. These olivine phenocrysts also show similarities with olivines from the EI Hierro basalts, which have been explained as being derived from partial melting of peridotite-pyroxenite lithologies (Gurenko et al., 2009). This is also consistent with previous studies about Shuangliao basalts in Northeastern China, which are considered to be derived from heterogeneous asthenosphere consisting of fusible pyroxenite/eclogite components related to subduction of the Pacific plate (Xu et al., 2012; Chen et al., 2015). The comparable ranges of Mn, Ca, Ni and Fe/Mn for olivine phenocrysts from both the North and the South CVB suggest that they may have been derived from hybrid mantle sources containing similar proportions of peridotite and pyroxenite/eclogite components (Fig. 4).

Although the above data support the recycled oceanic crust (in the form of pyroxenite/eclogite) in the mantle source of the North and the South CVB basaltic lavas, the following evidence shows that it was only a minor component in the source region. Fig. 9 shows that all the CVB samples match well with partial melting of a peridotitic source. Basanites and alkali basalts from the North CVB can be explained by low degrees (2.5–8%) of partial melting. Alkali basalts, tholeiites and basaltic andesites from the South CVB can be attributed to higher degrees (5–25%) of partial melting. This implies that the partial melting process governs the variations of REE (Rare Earth Element). In addition, we speculate that there is a possible relationship between partial melting degrees and lithospheric thickness. The North CVB samples that erupted on a thick lithosphere (100–120 km, Zhang et al., 2014) underwent low melting degrees and were dominated by alkali lavas with high La/Sm, and low Sm/Nd and SiO_2. In contrast, the South CVB samples that erupted on a thin lithosphere (60–80 km, Zheng et al., 2011) underwent moderate to high melting degrees and consist of both alkali and tholeiitic lavas with relatively low La/Sm, and high Sm/Nd and SiO_2.

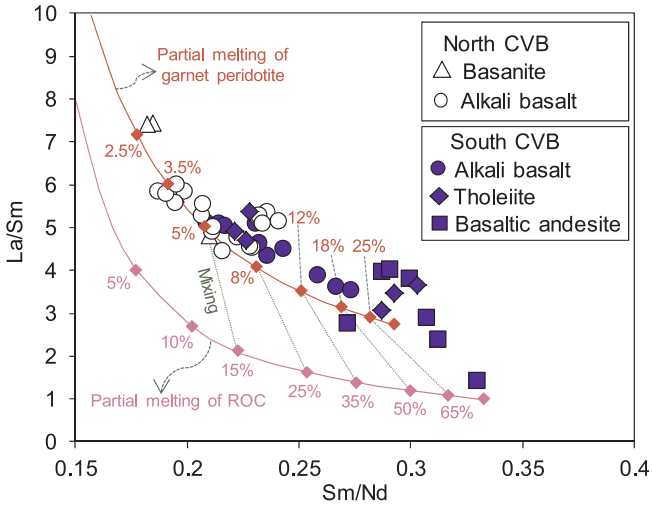

Fig. 9. Plot of Sm/Nd against La/Sm for the CVB basaltic lavas. Also shown are nonmodal batch partial melting of garnet peridotite (red solid line) and recycled oceanic crust (ROC, pink solid line). The modeling parameters are from Stracke et al. (2003). ROC is composed of 95% of subducted basalt and 5% of subducted sediment with 2.69 ppm La, 8.15 ppm Nd and 2.76 ppm Sm (Stracke et al., 2003). Numbers beside the batch melting curves represent variable degrees of partial melting. The green dashed lines represent binary mixing between ROC-derived melts and peridotite-derived melts. It is noted that samples that have experienced significant crustal contamination were excluded from this figure.

These observations indicate that the lithosphere influenced the geochemistry of the CVB basaltic lavas and can be attributed to the "Lid effect" (e.g., Humphreys and Niu, 2009; Niu et al., 2011; Davies et al., 2015). Based on statistical research on global geochemical variation in OIBs, Humphreys and Niu (2009) and Niu et al. (2011) have proposed that lithospheric thickness controls the final pressure of decompression melting and corresponding depth defines the bulk distribution

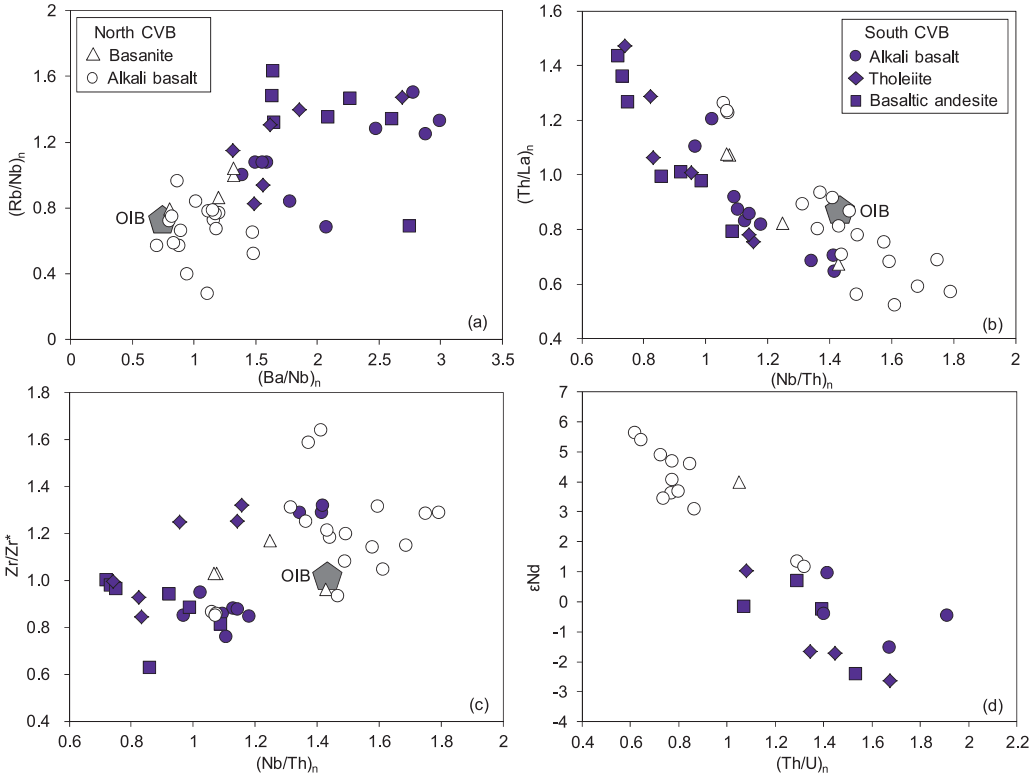

Fig. 10. Plots of $(Ba/Nb)_n$ vs. $(Rb/Nb)_n$ (a), $(Nb/Th)_n$ vs. $(Th/La)_n$ and $Zr/Zr^*(Zr_n/(Sm_n \times Nd_n)^{0.5})$ (b and c), and $(Th/U)_n$ vs. ε_{Nd} for the CVB basaltic lavas. It is noted that samples that have experienced significant crustal contamination were not included in this figure.

coefficients of elements in the source, which ultimately governs the geochemistry of OIBs (the so-called "Lid effect"). Basalts erupted on a thick lithosphere typically relate to high pressure and a low extent of melting of upwelling mantle and display low SiO_2, and high La/Sm and Sm/Nd. In contrast, those erupted on a thin lithosphere are generated by low mean pressure and a high extent of melting and are characterized by high SiO_2, and low La/Sm and Sm/Nd. It should be pointed out that the lithosphere thickness obtained according to the seismic data only reflects the present-day state of the mantle lithosphere in the studied area. It may be different from that at the ages of our samples (16–1 Ma).

However, variations of Sr—Nd—Hf isotopic compositions and some trace element ratios (such as Rb/Nb, Ba/Nb, Th/La, Nb/Th, Zr/Zr^* and Th/U) for the CVB samples cannot be attributed to partial melting processes under variable conditions but may reflect their source heterogeneity. For example, the North CVB basalts show OIB-like trace element ratios (such as Rb/Nb, Ba/Nb, Th/La, Nb/Th, Zr/Zr^* and Th/U) and depleted isotopic compositions, regardless of lithological types (Fig. 10), suggesting the involvement of depleted source components. In contrast, basaltic samples from the South CVB are characterized by variable Rb/Nb, Ba/Nb, Th/La, Nb/Th, Zr/Zr^* and Th/U (Fig. 10), and variable Sr—Nd—Hf isotopic compositions from depleted to EM-I like, regardless of lithological types (Fig. 7), suggesting the involvement of both depleted and enriched source components. One possibility is that both enriched and depleted source components are from asthenospheric mantle. Depleted source components may represent typical peridotitic mantle. Enriched components may represent recycled continental crust or ancient marine sediments that exist as 'plums' or 'blobs' in the convective mantle (Zeng et al., 2011; Kuritani et al., 2011, 2013; Liu et al., 2015; Wang et al., 2017). In this scenario, such enriched materials should contribute more to the genesis of the basalts from the North CVB that erupted on a thicker lithosphere (Fig. 1c), because they are more fusible and start to melt at a deeper depth relative to typical mantle peridotite and contribute more to basalts generated beneath a thicker lithosphere (e.g., Sobolev et al., 2007). This is apparently the opposite of what we observed in the samples from the North and the South CVB. Moreover, the coupled Hf—Nd isotopic compositions of basalts from the South CVB (Fig. 7b) also preclude the possible involvement of significant marine sediments during magma generation because both modern and ancient marine sediments commonly display decoupled Hf—Nd isotopic compositions with high ε_{Nd} and low ε_{Hf} values compared with the mantle array (e.g., Chauvel et al., 2008). We argue that melting of upwelling asthenosphere containing recycled continental crust or marine sediments cannot explain variations of isotopic compositions and trace element ratios for the CVB samples.

As discussed earlier, olivine phenocrysts from the North and the South CVB with similar Mn, Ni and Fe/Mn ratios at a given Fo (Fig. 4) support similar proportions of pyroxenite/eclogite components in the sources of the North and the South CVB basalts. If these pyroxenite/eclogite components derived from the subducted Pacific slab (Xu et al., 2012; Li et al., 2016; Chen et al., 2017; Choi et al., 2017), this implies that the chemical differences between the South and the North CVB basalts cannot be explained by different contributions of the Pacific slab materials during magma generation. Moreover, enriched source materials that contributed to the generation of the South CVB basalts are not likely related to the subducted Pacific slab (or the earlier Farallon-Izanagi slab) because the subduction of the Farallon-Izanagi plate or the Pacific plate happened since the late Mesozoic Era (Maruyama et al., 1997; Sun et al., 2007) and thus there is not enough time for the evolution of enriched isotopic signatures after such events.

We therefore propose that the depleted source components are from the asthenosphere, while the EM1-like enriched components are likely from the base of the sub-continental lithospheric mantle (SCLM) that has experienced ancient metasomatism. Information about the composition of the lithospheric mantle beneath the CVB is available from previous studies on the spinel peridotite xenoliths hosted in the Cenozoic alkali basalts from Huinan, Wangqing, Jiaohe, Shuangliao, Yong'an and Wudalianchi (Xu et al., 1998, 2003; Zhang et al., 2000; Wu

et al., 2003; Yu et al., 2009, 2012). The SCLM in northeastern China is essentially Proterozoic in age according to Re-Os isotopic compositions of peridotite xenoliths (Wu et al., 2003; Yu et al., 2012). These xenoliths are anhydrous and lack metasomatic phases such as amphibole and phlogopite. A large proportion of these peridotite xenoliths show variable enrichment of LILE with negative HFSE anomalies on the spider diagram plots (Xu et al., 1998, 2003; Yu et al., 2009, 2012). The involvement of metasomatized peridotites in the genesis of the South CVB basalts can therefore explain HFSE depletion (lower Zr/Zr^*, Nb/Th, Hf/Sm, Fig. 10c) and LILE enrichment (higher Rb/Nb, Ba/Nb, Th/La, Fig. 10a and b). However, peridotite xenoliths cannot be regarded as a direct mantle source of the South CVB basaltic samples because they are all spinel peridotites rather than garnet peridotites, whereas samples from the South CVB display fractionated HREE with $(Gd/Yb)_n$ ranging from 1.8 to 4.9 which indicate residual garnet during partial melting. In addition, LILE-enriched peridotite xenoliths show more depleted Sr-Nd isotopic compositions ($^{87}Sr/^{86}Sr = 0.7030–0.7052$; $\varepsilon_{Nd} = -1.3 – +8.7$, Xu et al., 1998, 2003; Zhang et al., 2000; Yu et al., 2009, 2012) relative to the South CVB basalts ($^{87}Sr/^{86}Sr = 0.7038–0.7053$; $\varepsilon_{Nd} = -2.6 – +3.1$). To resolve these discrepancies, we speculate that the basal SCLM beneath the South CVB is dominated by garnet peridotite with more enriched chemical compositions compared with shallower spinel peridotite, given that mantle metasomatism is far more significant at the interface between the base of lithosphere and the seismic low-velocity zone atop asthenosphere relative to the lithospheric mantle at shallow level (e.g., Humphreys and Niu, 2009). Infiltration and mixing of asthenosphere-derived small volume melts enriched in volatiles (e.g., H_2O and CO_2) and incompatible elements with depleted mantle peridotite would generate an enriched peridotite source which can evolve to an EM-1 isotopic signature, provided that there is enough time for the evolution of isotopic signatures after the metasomatic event (Pilet et al., 2005). Such metasomatized garnet peridotites were later eroded during lithosphere-asthenosphere interaction and contributed to the genesis of the South CVB basaltic lavas during lithosphere-asthenosphere interaction.

5.3. A model for the spatial distribution of basalts from the CVB

To account for spatial compositional variations of the late Cenozoic basaltic lavas from the CVB, we propose a model including dynamic melting of heterogeneous asthenospheric mantle and asthenosphere-lithosphere interaction induced by subduction of the Pacific plate (Fig. 11). The subducting Pacific slab became stagnant in the mantle transition zone at depths of 410–660 km beneath eastern China (Fig. 11a, e.g., Fukao et al., 1992; Huang and Zhao, 2006). The upper mantle above this stagnant Pacific slab may have formed a large mantle wedge where oceanic subduction and convective circulation induced back-arc extension, continental rifting and upwelling of asthenospheric mantle in eastern China (Fig. 11a, e.g., Huang and Zhao, 2006; Zhao and Ohtani, 2009). Interaction between lithosphere and upwelling asthenosphere created a “plum-pudding” type convective mantle. The extent of lithosphere extension and thinning is likely heterogeneous in space (Fig. 11b). Geophysical data have demonstrated that thickness of the present-day lithosphere beneath the South CVB is between 60 and

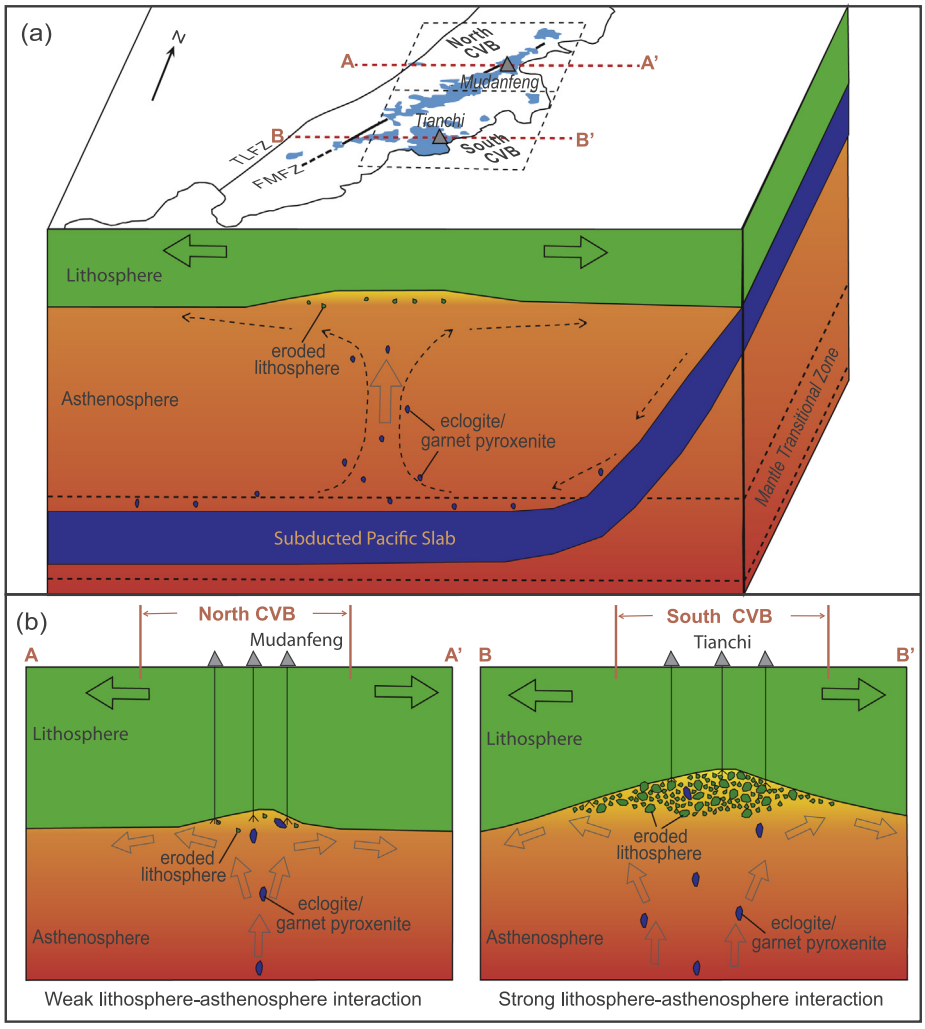

Fig. 11. Cartoon illustrating the proposed model accounting for the spatial distribution of the CVB basaltic lavas. (a) The subduction of Pacific plate underneath the Asian continent resulted in upper mantle convection and back-arc extension. The upwelling mantle flux consists of garnet pyroxenite/eclogite which may be derived from the stagnant oceanic slab in the mantle transition zone. The interaction between lithosphere and upwelling asthenosphere created a plum-pudding type convective mantle which acted as the magma source of the CVB basalts. (b) Schematic lithospheric profiles along the lines shown in Fig. 11a. Larger degrees of lithospheric erosion occurred beneath the South CVB due to more severe extension and lithosphere-asthenosphere interaction.

80 km (Fig. 1c, Zheng et al., 2011). In contrast, the lithosphere beneath the North CVB is much thicker (Fig. 1c, 100–120 km, Zhang et al., 2014). Such differences in thickness are likely due to variable degrees of extension and lithosphere-asthenosphere interaction by means of thermo-mechanical erosion (e.g., Davis, 1991). In this model, the ambient temperature of the basal SCLM was raised due to infiltration of asthenosphere-derived small melt fractions that acted as an agent for advectively transporting heat upwards to the lithosphere (Chung et al., 1994). This was followed by a progressive erosion of the basal SCLM through multiple thermo-mechanical processes accompanying convective upwelling of the asthenosphere. Consequently, the basal SCLM beneath the South CVB was gradually replaced by a 'plum-pudding'-type convecting mantle which mixed material from the SCLM (the 'plums') with the asthenospheric matrix (the 'pudding', Fig. 11b).

The basaltic samples from the South CVB with higher Sm/Nd, SiO_2, and lower La/Sm, and more enriched Sr−Nd−Hf isotope compositions, and variable degrees of HFSE depletion (Figs. 9 and 10) can thus be explained by larger melting degrees of asthenosphere at a shallower depth involving a larger amount of eroded, metasomatized lithospheric mantle due to asthenosphere-lithosphere interaction. In contrast, the much thicker lithosphere beneath the North CVB indicates relatively limited lithosphere-asthenosphere interaction and lithospheric thinning (Fig. 11b). Basalts from the North CVB are thus primarily produced by low melting degrees of asthenospheric mantle at high depths without significant contribution of lithospheric mantle materials. The upwelling asthenospheric materials consisting of predominantly typical mantle peridotite and dispersed garnet pyroxenite veins or blobs possibly derived from the stagnant Pacific slab in the mantle transition zone (e.g., Zhang et al., 2009; Yu et al., 2010; Xu et al., 2012; Li et al., 2016; Zhang and Guo, 2016; Chen et al., 2017), likely contributed equally to the genesis of the basaltic lavas from both the North and the South CVB.

6. Concluding remarks

The late Cenozoic basalts in the CVB delineate a remarkable composition-space variation pattern. The North CVB is dominated by basanites and alkali basalts with depleted Sr−Nd−Hf isotopic compositions, which may have been derived from low partial melting degrees at high depths of depleted source materials from the asthenospheric mantle consisting of peridotite and garnet pyroxenite. On the other hand, the South CVB consists of both alkali and sub-alkali basaltic lavas with highly variable Sr−Nd−Hf isotopic compositions from depleted to enriched, which may have been produced by larger degrees of partial melting of asthenospheric mantle at shallower depths. This involved a large amount of eroded, metasomatized lithospheric mantle formed as a result of asthenosphere-lithosphere interaction. We propose that decompression melting of upwelling asthenosphere and mechanical-chemical erosion of basal lithosphere related to lithosphere-asthenosphere interaction responsible for the genesis of the CVB magmas were likely associated with upper mantle convection and back-arc extension induced by deep subduction of the Pacific plate and its stagnancy in the transition zone.

Acknowledgments

We thank Prof. Chusi Li for the assistance in analysis of mineral compositions. This study was funded by the strategic priority research program (B) of the Chinese Academy of Sciences (XDB18000000), NSFC (41573009; 41373042, 41203031), Open Research Fund of the State Key Laboratory of Ore Deposit Geochemistry of China (SKLODG grant #201204). We greatly appreciate Dr. Pengyuan Guo and an anonymous reviewer for their constructive reviews and Professor Jinhui Yang for his diligent editorial handling.

References

Arndt, N.T., Christensen, U., 1992. The role of lithospheric mantle in continental flood volcanism: Thermal and geochemical constraints. J. Geophys. Res. Solid Earth 97 (B7), 10967–10981.
Ballentine, C.J., Lee, D.C., Halliday, A.N., 1997. Hafnium isotopic studies of the Cameroon line and new HIMU paradoxes. Chem. Geol. 139, 111–124.
Basu, A.R., Junwen, W., Wankang, H., Guanghong, X., Tatsumoto, M., 1991. Major element, REE, and Pb, Nd and Sr isotopic geochemistry of Cenozoic volcanic rocks of eastern China: implications for their origin from suboceanic-type mantle reservoirs. Earth Planet. Sci. Lett. 105, 149–169.
Chauvel, C., Blichert-Toft, J., 2001. A hafnium isotope and trace element perspective on melting of the depleted mantle. Earth Planet. Sci. Lett. 190, 137–151.
Chauvel, C., Lewin, E., Carpentier, M., Arndt, N.T., Marini, J.-C., 2008. Role of recycled oceanic basalt and sediment in generating the Hf–Nd mantle array. Nat. Geosci. 1, 64–67.
Chen, Y., Zhang, Y., Graham, D., Su, S., Deng, J., 2007. Geochemistry of Cenozoic basalts and mantle xenoliths in Northeast China. Lithos 96, 108–126.
Chen, L.H., Zeng, G., Jiang, S.Y., Hofmann, A.W., Xu, X.S., Pan, M.-B., 2009. Sources of Anfengshan basalts: Subducted lower crust in the Sulu UHP belt, China. Earth Planet. Sci. Lett. 286, 426–435.
Chen, H., Xia, Q.K., Ingrin, J., Jia, Z.B., Feng, M., 2015. Changing recycled oceanic components in the mantle source of the Shuangliao Cenozoic basalts, NE China: New constraints from water content. Tectonophysics 650, 113–123.
Chen, H., Xia, Q.K., Ingrin, J., Deloule, E., Bi, Y., 2017. Heterogeneous source components of intraplate basalts from NE China induced by the ongoing Pacific slab subduction. Earth Planet. Sci. Lett. 459, 208–220.
Choi, H.O., Choi, S.H., Schiano, P., Cho, M., Cluzel, N., Devidal, J.L., Ha, K., 2017. Geochemistry of olivine-hosted melt inclusions in the Baekdusan (Changbaishan) basalts: Implications for recycling of oceanic crustal materials into the mantle source. Lithos 284–285, 194–206.
Chung, S.L., Sun, S.S., Tu, K., Chen, C.H., Lee, C.Y., 1994. Late Cenozoic basaltic volcanism around the Taiwan Strait, SE China: product of lithosphere-asthenosphere interaction during continental extension. Chem. Geol. 112, 1–20.
Davis, P.M., 1991. Continental rift structures and dynamics with reference to teleseismic studies of the Rio Grande and East African rifts. Tectonophysics 197, 309–325.
Davies, D.R., Rawlinson, N., Laffaldano, G., Campbell, I.H., 2015. Lithospheric controls on magma composition along Earth's longest continental hotspot track. Nature 525, 511–514.
Deniel, C., Pin, C., 2001. Single-stage method for the simultaneousisolation of lead and strontium from silicate samples for isotopic measurements. Anal. Chim. Acta 426, 95–103.
Eggins, S.M., Woodhead, J.D., Kinsley, L.P.J., Mortimer, G.E., Sylvester, P., McCulloch, M.T., Hergt, J.M., Handler, M.R., 1997. A simple method for the precise determination of ≥ 40 trace elements in geological samples by ICPMS using enriched isotope internal standardisation. Chem. Geol. 134, 311–326.
Fan, Q., Hooper, P.R., 1989. The mineral chemistry of ultramafic xenoliths of eastern China: implications for upper mantle composition and the paleogeotherms. J. Petrol. 30, 1117–1158.
Fram, M.S., Lesher, C.E., 1993. Geochemical constraints on mantle melting during creation of the North Atlantic basin. Nature 363, 712–715.
Frey, F., Green, D., Roy, S., 1978. Integrated models of basalt petrogenesis: a study of quartz tholeiites to olivine melilitites from south eastern Australia utilizing geochemical and experimental petrological data. J. Petrol. 19, 463–513.
Fukao, Y., Obayashi, M., Inoue, H., Nenbai, M., 1992. Subducting slabs stagnant in the mantle transition zone. J. Geophys. Res. Solid Earth 97, 4809–4822.
Ghiorso, M.S., Sack, R.O., 1995. Chemical mass transfer in magmatic processes IV. A revised and internally consistent thermodynamic model for the interpolation and extrapolation of liquid-solid equilibria in magmatic systems at elevated temperatures and pressures. Contrib. Miner. Petrol. 119, 197–212.
Guo, P., Niu, Y., Ye, L., Liu, J., Sun, P., Cui, H., Zhang, Y., Gao, J., Su, L., Zhao, J., 2014. Lithosphere thinning beneath west North China Craton: evidence from geochemical and Sr–Nd–Hf isotope compositions of Jining basalts. Lithos 202, 37–54.
Gurenko, A.A., Sobolev, A.V., Hoernle, K.A., Hauff, F., Schmincke, H.-U., 2009. Enriched, HIMU-type peridotite and depleted recycled pyroxenite in the Canary plume: A mixed-up mantle. Earth Planet. Sci. Lett. 277, 514–524.
Hawkesworth, C.J., Marsh, J.S., Duncan, A.R., Erlank, A.J., Norry, M.J., 1984. The role of continental lithosphere in the generation of the Karoo volcanic rocks: evidence from combined Nd- and Sr-isotope studies. In: Erlank, A.J. (Ed.), Petrogenesis of the Volcanic Rocks of the Karoo Province, 13. Special Publication of Geological Society of South Africa, Johannesburg, pp. 341–354.
Herzberg, C., 2011. Identification of Source Lithology in the Hawaiian and Canary Islands: Implications for Origins. J. Petrol. 52, 113–146.
Hofmann, A., Jochum, K., Seufert, M., White, W., 1986. Nb and Pb in oceanic basalts: new constraints on mantle evolution. Earth Planet. Sci. Lett. 79, 33–45.
Hofmann, A.W., 1997. Mantle geochemistry: the message from oceanic volcanism. Nature 385, 219–229.
Hsu, C.N., Chen, J.C., 1998. Geochemistry of late Cenozoic basalts from Wudalianchi and Jingpohu areas, Heilongjiang Province, northeast China. J. Asian Earth Sci. 164, 385–405.
Hsu, C.N., Chen, J.C., Ho, K.S., 2000. Geochemistry of Cenozoic volcanic rocks from Kirin Province, northeast China. Geochem. J. 34, 33–58.
Huang, J., Li, S.G., Xiao, Y., Ke, S., Li, W.Y., Tian, Y., 2015. Origin of low δ^{26}Mg Cenozoic basalts from South China Block and their geodynamic implications. Geochim. Cosmochim. Acta 164, 298–317.

Huang, J., Zhao, D., 2006. High-resolution mantle tomography of China and surrounding regions. J. Geophys. Res. Solid Earth 111 (B09305).
Huang, X.L., Niu, Y., Xu, Y.G., Ma, J.L., Qiu, H.N., Zhong, J.W., 2013. Geochronology and geochemistry of Cenozoic basalts from eastern Guangdong, SE China: constraints on the lithosphere evolution beneath the northern margin of the South China Sea. Contrib. Miner. Petrol. 165, 437–455.
Humphreys, E.R., Niu, Y., 2009. On the composition of ocean island basalts (OIB): The effects of lithospheric thickness variation and mantle metasomatism. Lithos 112, 118–136.
Irvine, T.N., Baragar, W.R.A., 1971. A guide to the chemical classification of the common volcanic rocks. Can. J. Earth Sci. 8, 523–548.
Jahn, B.-M., Wu, F.-Y., Chen, B., 2000. Massive granitoids generation in Central Asia: Nd isotope evidence and implication for continental growth in the Phanerozoic. Episodes 23, 82–92.
Kogiso, T., Hirschmann, M.M., Frost, D.J., 2003. High-pressure partial melting of garnet pyroxenite: possible mafic lithologies in the source of ocean island basalts. Earth Planet. Sci. Lett. 216, 603–617.
Kuritani, T., Kimura, J.I., Miyamoto, T., Wei, H., Shimano, T., Maeno, F., Jin, X., Taniguchi, H., 2009. Intraplate magmatism related to deceleration of upwelling asthenospheric mantle: Implications from the Changbaishan shield basalts, northeast China. Lithos 112, 247–258.
Kuritani, T., Ohtani, E., Kimura, J.-I., 2011. Intensive hydration of the mantle transition zone beneath China caused by ancient slab stagnation. Nat. Geosci. 4, 713–716.
Kuritani, T., Kimura, J.-I., Ohtani, E., Miyamoto, H., Furuyama, K., 2013. Transition zone origin of potassic basalts from Wudalianchi volcano, northeast China. Lithos 156, 1–12.
Langmuir, C.H., Klein, E.M., Plank, T., 1992. Petrological systematics of mid-ocean ridge basalts: constraints on melt generation beneath ocean ridges. In: Morgan, J.P., Blackman, D.K., Sinton, J.M. (Eds.), Mantle Flow and Melt Generation at Mid-Ocean Ridges, Geophys Monogr Series. AGU (American Geophysic Union), Washington DC, pp. 81–180.
Le Bas, M.J., Le Maitre, R.W., Streckeisen, A., Zanettin, B., 1986. A chemical classification of volcanic rocks based on the total alkali-silica diagram. J. Petrol. 27, 745–750.
Li, H.Y., Xu, Y.G., Ryan, J.G., Huang, X.L., Ren, Z.Y., Guo, H., Ning, Z.G., 2016. Olivine and melt inclusion chemical constraints on the source of intracontinental basalts from the eastern North China Craton: Discrimination of contributions from the subducted Pacific slab. Geochim. Cosmochim. Acta 178, 1–19.
Li, S.G., Yang, W., Ke, S., Meng, X., Tian, H., Xu, L., He, Y., Huang, J., Wang, X.C., Xia, Q., Sun, W., Yang, X., Ren, Z.-Y., Wei, H., Liu, Y., Meng, F., Yan, J., 2017. Deep carbon cycles constrained by a large-scale mantle Mg isotope anomaly in eastern China. Natl. Sci. Rev. 4, 111–120. http://dx.doi.org/10.1093/nsr/nww070.
Liu, R.X., Chen, W.J., Sun, J.Z., Li, D.M., 1992a. The K-Ar age and tectonic environment of Cenozoic volcanic rock in China. In: Liu, R.X. (Ed.), The Age and Geochemistry of Cenozoic Volcanic Rock in China. Seismologic Press, Beijing, pp. 1–43 (in Chinese).
Liu, D., Nutman, A., Compston, W., Wu, J., Shen, Q.H., 1992b. Remnants of≥ 3800 Ma crust in the Chinese part of the Sino-Korean craton. Geology 20, 339–342.
Liu, C.Q., Masuda, A., Xie, G.H., 1994. Major-and trace-element compositions of Cenozoic basalts in eastern China: petrogenesis and mantle source. Chem. Geol. 114, 19–42.
Liu, J.Q., 1987. Study on geochronology of the Cenozoic volcanic rocks in northeastern China. Acta Petrologica 4, 21–31 (in Chinese).
Liu, J.Q., 1999. Chinese Volcanos. Science Press, Beijing (in Chinese).
Liu, J., Xia, Q.K., Deloule, E., Chen, H., Feng, M., 2015. Recycled oceanic crust and marine sediment in the source of alkali basalts in Shandong, eastern China: Evidence from magma water content and oxygen isotopes. J. Geophys. Res. Solid Earth 120, 8281–8303.
Liu, J.Q., Chen, L.H., Zeng, G., Wang, X.J., Zhong, Y., Yu, X., 2016. Lithospheric thickness controlled compositional variations in potassic basalts of Northeast China by melt-rock interactions. Geophys. Res. Lett. 43, 2582–2589.
Liu, J.Q., Chen, L.H., Wang, X.J., Zhong, Y., Yu, X., Zeng, G., Erdmann, S., 2017. The role of melt-rock interaction in the formation of Quaternary high-MgO potassic basalt from the Greater Khingan Range, northeast China. J. Geophys. Res. Solid Earth 122, 262–280.
Ma, L.F., Qiao, X.F., Min, L.R., Fan, B.X., Ding, X.Z. (Eds.), 2002. Geology Maps of China. Geology Press, Beijing, pp. 348 (in Chinese).
Maruyama, S., Isozaki, Y., Kimura, G., Terabayashi, M., 1997. Paleogeographic maps of the Japanese Islands: plate tectonic synthesis from 750 Ma to the present. Isl. Arc 6, 121–142.
McKenzie, D., Bickle, M.J., 1988. The volume and composition of melt generated by extension of the lithosphere. J. Petrol. 29, 625–679.
Míková, J., Denková, P., 2007. Modified chromatographic separation scheme for Sr and Nd isotope analysis in geological silicate samples. J. Geosci. 52, 221–226.
Niu, Y., 2005. Generation and evolution of basaltic magmas: some basic concepts and a new view on the origin of Mesozoic-Cenozoic basaltic volcanism in eastern China. Geol. J. China Universities 11, 9–46.
Niu, Y., Wilson, M., Humphreys, E.R., O'hara, M.J.., 2011. The origin of intra-plate ocean island basalts (OIB): the lid effect and its geodynamic implications. J. Petrol. 52, 1443–1468.
Okamura, S., Arculus, R.J., Martynov, Y.A., 2005. Cenozoic Magmatism of the North-Eastern Eurasian margin: The role of lithosphere versus asthenosphere. J. Petrol. 46, 221–253.
Pilet, S., Hernandez, J., Sylvester, P., Poujol, M., 2005. The metasomatic alternative for ocean island basalt chemical heterogeneity. Earth Planet. Sci. Lett. 236, 148–166.
Pin, C., Zalduegui, J.S., 1997. Sequential separation of light rare-earth elements, thorium and uranium by miniaturized extraction chromatography: Application to isotopic analyses of silicate rocks. Anal. Chim. Acta 339, 79–89.
Qin, X.F., 2008. Geochronology and Geochemistry of Tertiary basalts from Mudanjiang-Mishan area, Northeast China: Mantle sources and tempo-spatial variations. Ph.D. dissertation. Graduate School of China Academy of Sciences. Beijing (in Chinese with English abstract).
Qin, X.F., Xu, Y.G., Zhang, H.H., Yu, S.Y., Qiu, H.N., 2008. Petrogenetic diversity of continental subalkaline volcanic rocks: An example from the Dunhua-Mishan-Dongning volcanic belt. Acta Petrologica Sinica 24, 2501–2514 (in Chinese with English abstract).
Rudnick, R.L., Fountain, D.M., 1995. Nature and composition of the continental crust: a lower crustal perspective. Rev. Geophys. 33, 267–309.
Sakuyama, T., Tian, W., Kimura, J.-I., Fukao, Y., Hirahara, Y., Takahashi, T., Senda, R., Chang, Q., Miyazaki, T., Obayashi, M., Kawabata, H., Tatsumi, Y., 2013. Melting of dehydrated oceanic crust from the stagnant slab and of the hydrated mantle transition zone: constraints from Cenozoic alkaline basalts in eastern China. Chem. Geol. 359, 32–48.
Sobolev, A.V., Hofmann, A.W., Kuzmin, D.V., Yaxley, G.M., Arndt, N.T., Chung, S.L., Danyushevsky, L.V., Elliott, T., Frey, F.A., Garcia, M.O., Gurenko, A.A., Kamenetsky, V.S., Kerr, A.C., Krivolutskaya, N.A., Matvienkov, V.V., Nikogosian, I.K., Rocholl, A., Sigurdsson, I.A., Sushchevskaya, N.M., Teklay, M., 2007. The amount of recycled crust in sources of mantle-derived melts. Science 316, 412–417.
Sobolev, A.V., Hofmann, A.W., Sobolev, S.V., Nikogosian, I.K., 2005. An olivine-free mantle source of Hawaiian shield basalts. Nature 434, 590–597.
Stracke, A., Bizimis, M., Salters, V.J.M., 2003. Recycling oceanic crust: Quantitative constraints. Geochem. Geophys. Geosyst. 4, 8003. http://dx.doi.org/10.1029/2001GC000223.
Sun, S.S., McDonough, W.F., 1989. Chemical and isotopic systematics of oceanic basalts: implications for mantle composition and processes. In: Saunders, A.D., Norry, M.J. (Eds.), Magmatism in the Ocean Basins. Geological Socity Special Publication, pp. 313–345.
Sun, W., Ding, X., Hu, Y.-H., Li, X.-H., 2007. The golden transformation of the Cretaceous plate subduction in the west Pacific. Earth Planet. Sci. Lett. 262, 533–542.
Tanaka, T., Togashi, S., Kamioka, H., Amakawa, H., Kagami, H., Hamamoto, T., Yuhara, M., Orihashi, Y., Yoneda, S., Shimizu, H., 2000. JNdi-1: a neodymium isotopic reference in consistency with LaJolla neodymium. Chem. Geol. 168, 279–281.
Tang, Y., Obayashi, M., Niu, F., Grand, S.P., Chen, Y.J., Kawakatsu, H., Tanaka, S., Ning, J., Ni, J.F., 2014. Changbaishan volcanism in northeast China linked to subduction-induced mantle upwelling. Nat. Geosci. 7, 470–475.
Tatsumoto, M., Basu, A.R., Wankang, H., Junwen, W., Guanghong, X., 1992. Sr, Nd, and Pb isotopes of ultramafic xenoliths in volcanic rocks of Eastern China: enriched components EMI and EMII in subcontinental lithosphere. Earth Planet. Sci. Lett. 113, 107–128.
Tian, H.C., Yang, W., Li, S.G., Ke, S., Chu, Z.Y., 2016. Origin of low δ 26 Mg basalts with EM-I component: Evidence for interaction between enriched lithosphere and carbonated asthenosphere. Geochim. Cosmochim. Acta 188, 93–105.
Wang, X.C., Li, Z.X., Li, X.H., Li, J., Liu, Y., Long, W.G., Zhou, J.B., Wang, F., 2012. Temperature, pressure, and composition of the mantle source region of late cenozoic basalts in Hainan Island, SE Asia: a consequence of a young thermal mantle plume close to subduction zones? J. Petrol. 53, 177–233.
Wang, X.C., Li, Z.X., Li, X.H., Li, J., Xu, Y.G., Li, X.H., 2013. Identification of an ancient mantle reservoir and young recycled materials in the source region of a young mantle plume: Implications for potential linkages between plume and plate tectonics. Earth Planet. Sci. Lett. 377–378, 248–259.
Wang, X.C., Wilde, S.A., Li, Q.L., Yang, Y.N., 2015. Continental flood basalts derived from the hydrous mantle transition zone. Nat. Commun. 6, 7700.
Wang, X.J., Chen, L.H., Hofmann, A.W., Mao, F.G., Liu, J.Q., Zhong, Y., Xie, L.W., Yang, Y.H., 2017. Mantle transition zone-derived EM1 component beneath NE China: Geochemical evidence from Cenozoic potassic basalts. Earth Planet. Sci. Lett. 465, 16–28.
Wang, Y., Li, C., Wei, H., Shan, X., 2003. Late Pliocene–recent tectonic setting for the Tianchi volcanic zone, Changbai Mountains, northeast China. J. Asian Earth Sci. 21, 1159–1170.
Wei, H., Wang, Y., Jin, J., Gao, L., Yun, S.H., Jin, B., 2007. Timescale and evolution of the intracontinental Tianchi volcanic shield and ignimbrite-forming eruption, Changbaishan, Northeast China. Lithos 96, 315–324.
Wu, F.Y., Walker, R.J., Ren, X.Y., Sun, D.Y., Zhou, X.H., 2003. Osmium isotopic constraints on the age of lithospheric mantle beneath northeastern China. Chem. Geol. 196, 107–129.
Xu, Y.G., Menzies, M.A., Vroon, P., Mercier, J.-C., Lin, C., 1998. Texture–temperature–geochemistry relationships in the upper mantle as revealed from spinel peridotite xenoliths from Wangqing, NE China. J. Petrol. 39, 469–493.
Xu, Y.G., Menzies, M.A., Thirlwall, M.F., Huang, X.L., Liu, Y., Chen, X.M., 2003. "Reactive" harzburgites from Huinan, NE China: products of the lithosphere-asthenosphere interaction during lithospheric thinning? Geochim. Cosmochim. Acta 67, 487–505.
Xu, Y.G., Zhang, H.H., Qiu, H.N., Ge, W.C., Wu, F.Y., 2012. Oceanic crust components in continental basalts from Shuangliao, Northeast China: Derived from the mantle transition zone? Chem. Geol. 328, 168–184.
Yan, J., Zhao, J.X., 2008. Cenozoic alkali basalts from Jingpohu, NE China: the role of lithosphere–asthenosphere interaction. J. Asian Earth Sci. 33, 106–121.
Yang, W., Teng, F.Z., Zhang, H.F., Li, S.G., 2012. Magnesium isotopic systematics of continental basalts from the North China craton: Implications for tracing subducted carbonate in the mantle. Chem. Geol. 328, 185–194.
Yu, X., Chen, L.H., Zeng, G., 2015a. Growing magma chambers control the distribution of small-scale flood basalts. Sci. Rep. 5, 16824. http://dx.doi.org/10.1038/srep16824.
Yu, X., Lee, C.T.A., Chen, L.H., Zeng, G., 2015b. Magmatic recharge in continental flood basalts: Insights from the Chifeng igneous province in Inner Mongolia. Geochem. Geophys. Geosyst. 16, 2082–2096.

Yu, S.Y., Song, X., Xu, Y., Chen, L., Li, J., 2012. Effects of melt percolation on the Re-Os systematics of continental mantle lithosphere: A case study of spinel peridotite xenoliths from Heilongjiang, NE China. Science China: Earth Sciences 1–17.
Yu, S.Y., Xu, Y.G., Ma, J.L., Zheng, Y.F., Kuang, Y.S., Hong, L.B., Ge, W.C., Tong, L.X., 2010. Remnants of oceanic lower crust in the subcontinental lithospheric mantle: Trace element and Sr–Nd–O isotope evidence from aluminous garnet pyroxenite xenoliths from Jiaohe, Northeast China. Earth Planet. Sci. Lett. 297, 413–422.
Yu, S.Y., Xu, Y.G., Huang, X.L., Ma, J.L., Ge, W.C., Zhang, H.H., Qin, X.F., 2009. Hf-Nd isotopic decoupling in continental mantle lithosphere beneath Northeast China: Effects of pervasive mantle metasomatism. J. Asian Earth Sci. 35, 554–570.
Zeng, G., Chen, L.H., Xu, X.S., Jiang, S.Y., Hofmann, A.W., 2010. Carbonated mantle sources for Cenozoic intra-plate alkaline basalts in Shandong, North China. Chem. Geol. 273, 35–45.
Zeng, G., Chen, L.H., Hofmann, A.W., Jiang, S.Y., Xu, X.S., 2011. Crust recycling in the sources of two parallel volcanic chains in Shandong, North China. Earth Planet. Sci. Lett. 302, 359–368.
Zeng, G., Chen, L.H., Yu, X., Liu, J.Q., Xu, X.S., Erdmann, S., 2017. Magma-magma interaction in the mantle beneath eastern China. J. Geophys. Res. Solid Earth 122, 2763–2779.
Zhang, J.J., Zheng, Y.F., Zhao, Z.F., 2009. Geochemical evidence for interaction between oceanic crust and lithospheric mantle in the origin of Cenozoic continental basalts in east-central China. Lithos 110, 305–326.
Zhang, M., Guo, Z., 2016. Origin of Late Cenozoic Abaga-Dalinuoer basalts, eastern China: Implications for a mixed pyroxenite–peridotite source related with deep subduction of the Pacific slab. Gondwana Res. 37, 130–151.
Zhang, M., Suddaby, P., O'Reilly, S.Y., Norman, M., Qiu, J., 2000. Nature of the lithospheric mantle beneath the eastern part of the Central Asian fold belt: mantle xenolith evidence. Tectonophysics 328, 131–156.
Zhang, M., Suddaby, P., Thompson, R.N., Thirlwall, M.F., Menzies, M.A., 1995. Potassic volcanic rocks in NE China: geochemical constraints on mantle source and magma genesis. J. Petrol. 36, 1275–1303.
Zhang, R., Wu, Q., Sun, L., He, J., Gao, Z., 2014. Crustal and lithospheric structure of Northeast China from S-wave receiver functions. Earth Planet. Sci. Lett. 401, 196–205.
Zhang, Z.C., Feng, C.Y., Li, Z.N., Li, S.C., Xin, Y., Li, Z.M., Wang, X.Z., 2002. Petrochemical study of the Jingpohu Holocene alkali basaltic rocks, northeastern China. Geochem. J. 36, 133–153.
Zhao, D., Ohtani, E., 2009. Deep slab subduction and dehydration and their geodynamic consequences: evidence from seismology and mineral physics. Gondwana Res. 16, 401–413.
Zheng, Y., Shen, W., Zhou, L., Yang, Y., Xie, Z., Ritzwoller, M.H., 2011. Crust and uppermost mantle beneath the North China Craton, northeastern China, and the Sea of Japan from ambient noise tomography. J. Geophys. Res. Solid Earth 116 (B12312).
Zindler, A., Hart, S., 1986. Chemical Geodynamics. Annu. Rev. Earth Planet. Sci. 14, 493–571.
Zou, H., Zindler, A., Xu, X., Qi, Q., 2000. Major, trace element, and Nd, Sr and Pb isotope studies of Cenozoic basalts in SE China: mantle sources, regional variations, and tectonic significance. Chem. Geol. 171, 33–47.